CHARACTERIZATION OF POLYCRYSTALLINE SILICON GROWN IN A FLUIDIZED BED REACTOR

By

MEGAN MUREEN DAHL

A thesis submitted in partial fulfillment of the
requirements for the degree of

MASTER OF SCIENCE IN MATERIASL SCIENCE AND ENGINEERING

WASHINGTON STATE UNIVERSITY
School of Mechanical and Materials Engineering

May 2009

To the faculty of Washington State University:

The members of the Committee to examine the thesis of MEGAN MUREEN DAHL find it satisfactory and recommend that it be accepted.

_____
Chair

_____

_____

ACKNOWLEDGMENT

Thank you to everyone who made this project possible, namely Professors David Bahr, Grant Norton and David Field, as well as the graduate and undergraduate students who contributed, Aikaterini Bellou, Julie Reid, Mohamad Zbib, Nicole Overman, and Steve Letourneau at Boise State for his help and guidance on the TEM. I would also like to thank Wayne Osborne at REC Silicon for his enthusiastic help with this project because it would not have been possible without him. Of course, I would like to thank my husband, Randy, and family for providing support along the way with which I could not have done without.

Financial support was provided by REC Silicon, Inc.

CHARACTERIZATION OF POLYCRSYTALLINE SILICON GROWN IN A FLUIDIZED BED REACTOR

Abstract

By Megan Mureen Dahl, MS
Washington State University
May 2009

Chair: David F. Bahr

Due to an increase in demand for photovoltaic (PV) materials, the fluidized bed reactor (FBR) has become a popular alternative to the traditional and expensive method of producing and acquiring photovoltaic grade polycrystalline silicon (polysilicon). Traditional polysilicon acquisition for the PV industry relied on waste materials from the semiconductor industry that used the expensive Siemens reactor to produce the ultra pure silicon. Due to the recent application of fluidized bed technology to the silicon industry, it becomes necessary to characterize the product in order to fully understand its growth mechanisms as well as the most suitable handling techniques.

The fluidized bed reactor makes use of pyrolytic decomposition of silane gas onto seed particles to form high purity polysilicon. The polysilicon granules were analyzed with various characterization techniques to establish their macro and microstructures. Optical microscopy reveals a ringed structure with a closer electron microscopy examination detecting that the dark contrast rings consist of a less dense, porous structure. Transmission electron microscopy and X-Ray diffraction analysis determined that the as received silicon has an average grain size of 30 nm. A minor amount of grain

growth is observed with subsequent annealing cycles under 1050°C; significant abnormal grain growth is observed at higher annealing temperatures. Hardness data was collected to establish mechanical property details and their effects of annealing on them. Hardness of granules was determined to be approximately 10% less than that of single crystal material. Heat treatments had no significant effect on the hardness of the material at annealing times used in this thesis.

In addition to the polysilicon granules produced in the FBR, a homogeneously nucleated material referred to as fines is produced. Fines are often considered a parasitic material due to the consumption of silane gas to form the particles. Analysis of the fines by TEM and Fourier transform infrared (FTIR) spectroscopy reveals that the mean and median diameters are 78 nm and that the particles are hydrogenated amorphous silicon. Annealing these particles causes non-diffusion limited crystallization determined by crystallization vs. amorphous ratios of various sized particles.

Table of Contents

List of Figures

List of Tables

Chapter One: Introduction

1.1 Background and Motivation

The development of low-cost polycrystalline silicon technology has risen dramatically in conjunction with the market for photovoltaic (PV) materials.[1] Historically, silicon used in the PV industry has come from rejected semiconductor material,[2] but rising demands for this PV quality silicon has outstripped the available waste material. Efforts to discover an alternative method of polysilicon production are important due to the high cost of the traditional Siemens process that is used in the semiconductor industry. In order to supplement this growing industry, a popular alternative method, the fluidized bed reactor (FBR), has been developed; most recently the first large commercial scale FBR has been opened by REC Silicon in Moses Lake, WA. Because this method has only been explored in industry for under a decade, it is important to study and characterize the product to possibly improve efficiency of multiple aspects of the product both in terms of understanding materials growth processes and the resulting properties of the final product material.

There is significant literature documenting the microstructure and influences of heat treatments and growth conditions of thin and thick film silicon on substrates[3,4,5] and a growing amount of information on bulk polysilicon via the Siemens process;[6] however, there is very little to no information on FBR product. It becomes important then to detail the microstructure of as received and annealed samples to help provide insight into possible growth mechanisms of the material as well as mechanical properties that the

silicon may exhibit. For example, it has been observed that samples annealed at temperatures above 1050°C for 6 hours have a higher hardness than those in the as received state (Chapter 3). An added low-cost step may provide PV industries with a material that fractures with different stresses than the original granular product. In addition to the polysilicon granular product, the FBR also produces nm scale aerosol particles via homogeneous nucleation. There has been research documenting growth kinetics that relates the quantity of material produced to the input gasses[18, 19] however very little research has been performed on the material structure.

The purpose of this thesis is to characterize silicon grown by the FBR, including the microstructure in order to provide insight into handling techniques as well as to the growth methods in order to supply an even more efficient means of production in the future.

1.2 Polysilicon Production methods

The long established Siemens process was developed in the 1950's by the Siemens company in Germany. This method makes use of chemical vapor deposition (CVD) to grow polysilicon material onto seed rods. Traditionally, a purified silicon containing gas such as trichlorosilane ($SiHCl_3$) is introduced into a bell shaped chamber under vacuum in order to begin deposition at temperatures between 1100 and 1200°C (Figure 1. 1). Because the seed rods must be heated via resistance as a current is passed through the material, size constraints must be imposed. Generally these rods are up to 150cm in length and no more than 150mm in diameter.[2] Although it has been estimated that over 80% of the worldwide production of semiconductor grade silicon is produced in this manner, its major drawbacks include high energy consumption necessary to sustain

the process as well as a low silicon extraction yield (up to 60% in theory, but only 15-30% in practice).[2,7] Other problems with the Siemens process involve extensive corrosion of the reactor components due to the release of hydrogen chloride as a by-product of the chemical reaction, as well as the required long run time to achieve the final product. Improvements have been made to the method in a modified Siemens process that uses monosilane gas to reduce reaction temperatures to around 800°C; however most of the major drawbacks still exist.

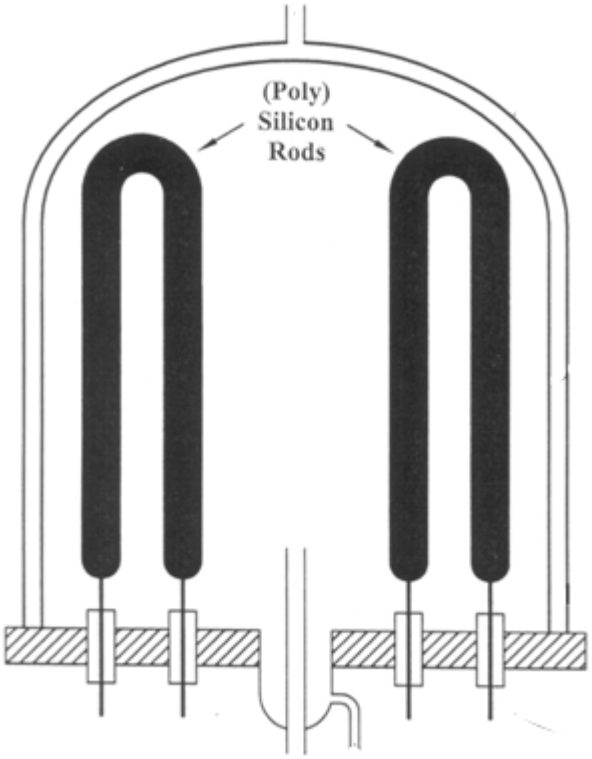

Figure 1. 1 Siemens reactor schematic.[8]

Due to the high energy consumption, relatively slow growth rates, and the highly corrosive environment created by the Siemens reactor, a low energy and low cost alternative method for producing polysilicon has been pursued. One of the most popular

methods is the fluidized bed reactor. Fluidized bed technology was first invented in the 1920's in Germany for coal gasification and metal refining applications.[9] It wasn't until the 1960's that silicon deposition was demonstrated in the FBR by using chlorosilane ($2HSiCl_3$) to produce semiconductor quality material.[10] Because the Siemens process became the standard for semiconductor silicon, the FBR was not investigated again for commercial applications again until the 1980's.[11-13] Full scale industrial silicon applications of FBR technology for PV quality silicon, however, were not recognized until the last decade.

The production of pure silicon in granular form is achieved by pyrolytic decomposition of silane gas inside of the reactor. Silicon seed material averaging 100 - 300μm in diameter (up to 2000 μm in literature)[11] is inserted into the bottom of the chamber before fluidization. Heated hydrogen is used to fluidize the material to provide two specific properties: the first is a perfectly isothermal state to assist in chemical reactions, and the second is to create ideal particle mixing to ensure uniform particle surface treatment.[14] In addition to hydrogen, other literature sources have used inert gasses such as argon, nitrogen or helium as the fluidizing gas. Temperature and time dependencies for aerosol particulate growth (discussed in chapter 4) have been found to correlate with the type of carrier gas used.[15]

The fluidized bed apparatus consists of a cylindrical reactor constructed of stainless steel with an inner diameter approximately 13 cm and a height of approximately 160 cm. An expansion zone located at the top of the reactor is roughly twice the diameter of the lower half and is used to allow the particles to drop back into the bed.[14, 12] The chamber is heated with an external heater to a temperature between 650 and 750°C; the

temperature varies along the column height. Gas inlets are located at the bottom of the reactor and the flow of process gasses, hydrogen and silane, is controlled by controlling the inlet mass flow conditions. The gasses are pre-heated to a temperature below silane pyrolysis before being injected into the reactor.[14] Silane concentrations of the feed gas between 10 and 60% by volume (with the balance H_2) have been tested; [12] the samples used in this current study are from intermediate silane concentrations in this range. Additionally, the concentration profile of silane most likely changes in the reactor as a function of column height as silicon is deposited and hydrogen is released. The reactor is kept fluidized by the use of multilayer screens. A mesh screen is supported by a thin stainless steel plate punctured with 0.5mm holes.[12] Fine particles are collected at the top of the reactor by passing through filters and cyclones, and the feed gas can be recycled in the process. Granular material is grown from the seed material for approximately one day in the reactor before reaching the predetermined size of particles used in this current study. Figure 1. 2 A is a simple schematic of the FBR setup and Figure 1. 2 B is representative of the silicon granular product.

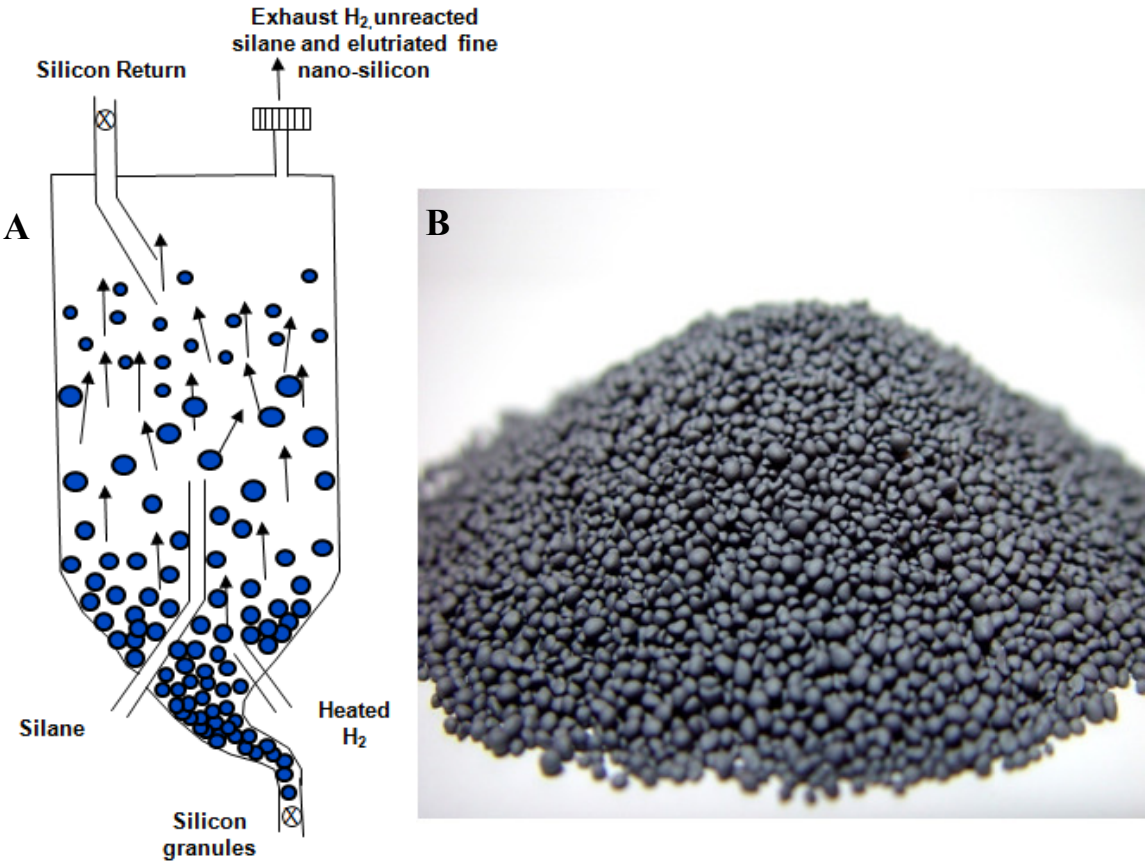

Figure 1. 2 A) Simple fluidized bed reactor schematic.[8] B) Silicon granular material.[8]

1.3 Other Material Produced in the Fluidized Bed Reactor

As previously stated, in addition to the granular polysilicon produced, aerosol particles (also referred to as fines), are homogeneously nucleated within the reactor and are found loose and on the reactor walls.[12,16] Because homogeneous reactions cause a reduction in available silane gas, this material is generally considered unwanted and parasitic, and has been linked to a lower granule yield.[2,7]

Homogenous nucleation was first studied in low pressure CVD reactors. Researchers found that a relationship between temperature and silane concentrations

exists that predicts when aerosol particles will from. A critical silane concentration was first recognized by Eversteijn in 1971 that was identified as dependent on temperature.[17] The critical silane concentration is defined as the concentration at which homogeneous nucleation occurs at a given temperature. In agreement, others found that at reasonably high temperatures, usually above 800°C, the critical silane concentrations could be relatively low. Authors, including Eversteijn have reported concentrations below 0.25% by volume are sufficient enough to begin the gas-phase nucleation as long as the temperatures are sufficiently high.[11, 15,17] In order for the low pressure CVD reactors to avoid excess aerosol generation, they are forced to run at low silane concentrations and limit the production of the polysilicon material. However, the FBR is able to run at much higher concentrations while avoiding massive quantities of aerosol particles. Some researchers believe this is possible due to two advantages: the first is that there is less free space for homogeneous reactions to take place in the reactor chamber, and the second is that the nucleated fines are scavenged and incorporated into the polysilicon.[12] The contribution of the gas-phase nucleated particles to the overall growth of the granules is debated and discussed in chapter 4 of this paper.

In addition to finding correlations between silane concentrations, temperatures, and aerosol production, other research has been performed to determine the kinetics of the reaction. Onischuk and his colleagues have performed numerous studies on characterizing the growth of the particles. To better understand the formation, Onischuk obtained the particles by thermal decomposition in a quartz flow reactor in argon. The decomposition is the same as in other literature, however it is done at much lower temperatures, between 550°C and 950°C and at very fast times, less than one second.[18]

By methods of Fourier transform infrared spectroscopy, hydrogen evolution, and TEM work, the researchers determined that the aerosol particles are hydrogenated amorphous silicon and are roughly 5-30nm in diameter. Kinetic modeling was based on the notion that the intermediate product reactions called silylenes (Si_nH_{2n}) are the components contributing to the solid particle growth rather than heterogeneous decomposition of the gassy intermediates of silane (SiH_4), disilane (Si_2H_6), and trisilane (Si_3H_8).[18,19] These results are based on the amount of hydrogen present in the particles and the known hydrogen content of the constituent parts.

1.3 Microstructures in Polysilicon

In thin and thick film polysilicon, the microstructure is characterized by not only the grain size, but also by the texture and grain distribution. All of these attributes are important for film applications in microelectronics as they affect mechanical and electronic properties, and are the cause for advanced research into growth mechanisms.[3] Thicknesses for thin films are generally considered to be between 0.1 and 0.5 μm, while thick films are larger than 0.5 μm. Ultra-thin polysilicon is also under current investigation and is considered to be less than 0.1 μm thick. For simplicity, the term thin films will be used to characterize the discussed microstructure. Due to the small height dimensions in thin films, surface energy becomes the major driving force for nucleation and growth. In bulk materials, the driving force for grain growth is usually due to other factors such as grain boundary energy.

Polysilicon thin films are usually created one of two ways: the first is to deposit polycrystalline silicon by means of CVD, or a variation of CVD onto a silicon oxide substrate, and the second way is to crystallize an amorphous layer on a substrate. In the

case with the crystallized amorphous layer, the grains may be only random in the homogeneously nucleated grains, where heterogeneously nucleation grains on the surface may favor a specific orientation and be nonrandom. As deposited films may also have orientation preferred grains and be nonrandom.[4] This becomes important as some orientations may favor extra grain growth called abnormal or secondary grain growth.

Secondary grain growth is often seen in polycrystalline thin films after high temperature (>1040°C) post-production heat treatments.[3] A fully crystallized film may undergo grain growth in which all normal grains grow at similar rates; however, secondary grain growth refers to the abnormal growth of a few grains that change at a faster rate by annihilating adjacent grains. These large abnormal grains are described as columnar and are much larger than the normal grains that are usually about the same size as the film thickness. Figure 1. 3 is a schematic of the differences in grain sizes between the normal and abnormal grains and Figure 1.4 is a TEM image of secondary grain growth in thin film polysilicon. Some secondary grains are outlined in black to emphasize the difference in size between the normal and abnormal grains.

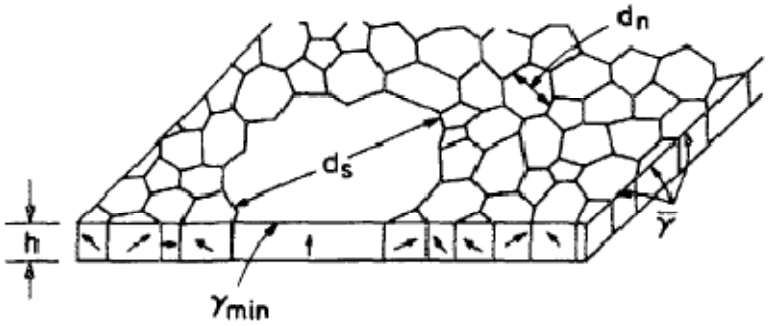

Figure 1. 3 Schematic of secondary grain within a normal grain matrix with a thickness h, an abnormal grain with size d_s, a normal grain size of d_n, and surface energies of the abnormal grain and normal grains, γ_{min} and γ, respectively.[4]

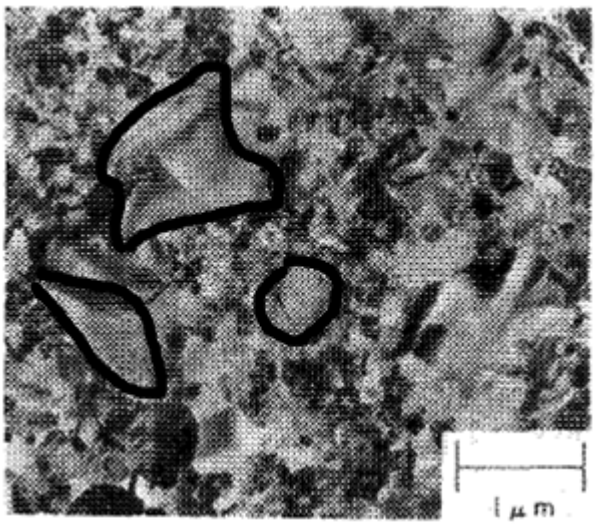

Figure 1. 4 TEM image of secondary or abnormal grain growth in a polysilicon thin film.[5]

The mechanism for growth in secondary grains is attributed to multiple energy reduction theories. The theory that contributes to most of the driving force is directed by surface energy anisotropy in which the energy of the system may be reduced by larger grains with preferential orientations that minimize the surface energy.[5] A more minor contributing theory involves a difference in dislocation densities between the normal and secondary grains.[3] The microstructure of polysilicon grown in the Siemens reactor has also been studied. Although widely used as the base material for the semiconductor industry, little research has been performed on the bulk structure. The material is rarely used in the raw form, and is generally used as the melt for the Czochralski or float zone methods in growing large single crystal ingots. However, like thin film polycrystalline, the microstructure has large effects on the properties of the material which may lead to better or worse handling methods. Unlike grains found in thin films, grain sizes found in the bulk material are on the scale of microns. In addition, the grains in the as received

material are long, slender, and parallel, where the overall structure appearance is "feather-like" (Figure 1. 5).[6,20] The difference in microstructures between thin film and bulk polysilicon could be due to multiple possibilities. First, the silicon is deposited onto a polycrystalline substrate instead of an amorphous oxide layer. This reduces the possibility of internal stresses that may influence grain growth. Second, the driving force has shifted away from surface anisotropy driven to bulk mechanisms.

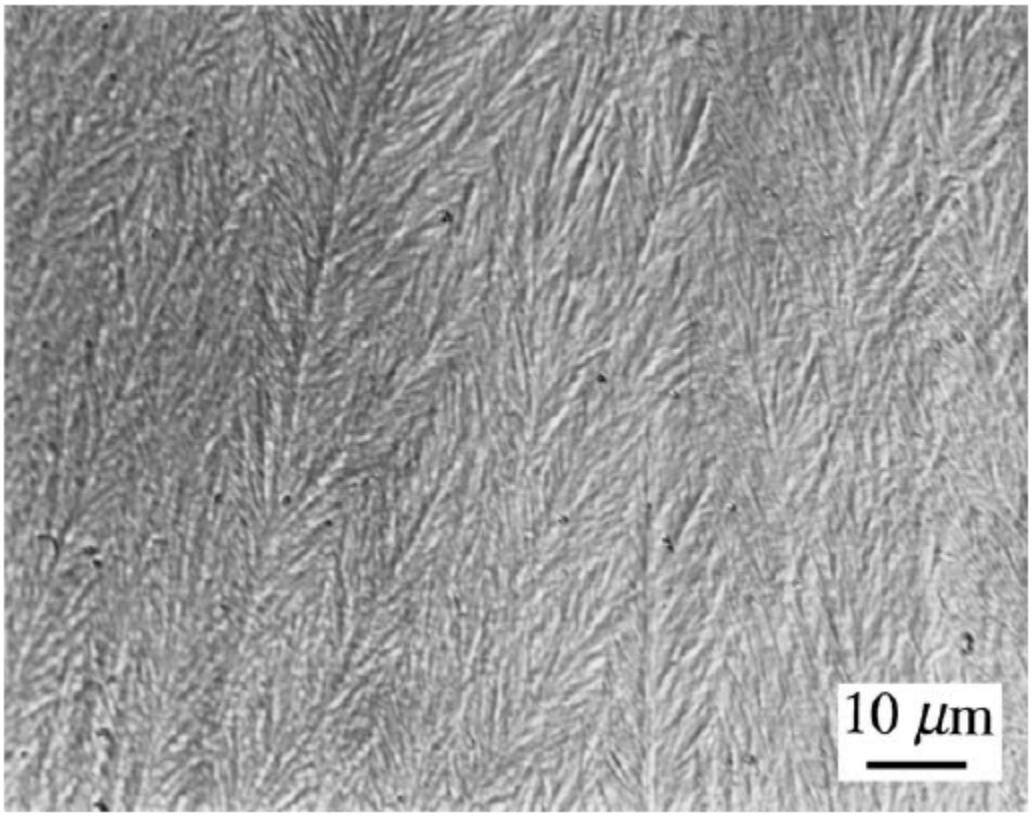

Figure 1. 5 Acicular grain appearance in polysilicon grown via the Siemens process.[6]

Subsequent annealing treatments reveal a structure change. At temperatures above 1375°C and times of 12 hours and longer, the elongated grains become equiaxed to a diameter roughly the same size as the smallest dimension of the feathered grains.

Intermediate temperatures reveal a structure that is primarily equiaxed with remnants of elongated grains within the matrix. The most interesting note, shown in Figure 1.6, is that at the high temperatures and long annealing times (up to 24 hours) the grains show no signs of secondary or abnormal grain growth that is found in thin films, regardless of the fact that the activation energy for diffusion across grain boundaries is similar to those values found in literature for thin films.[6]

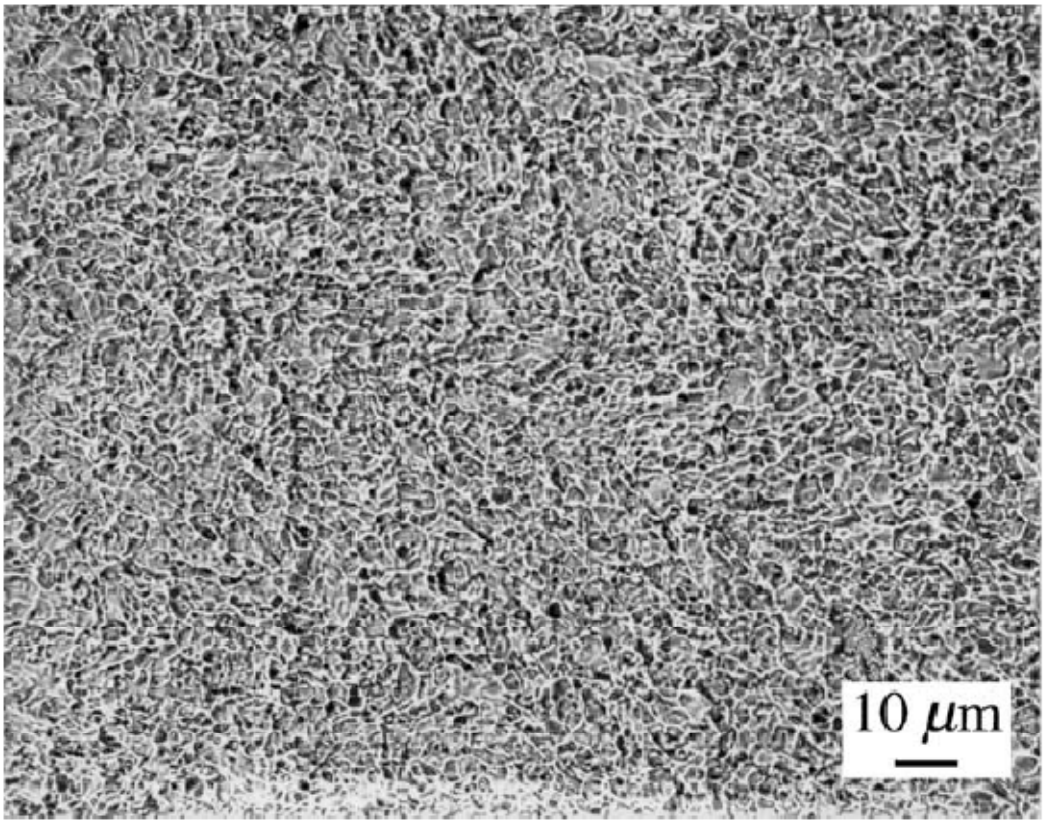

Figure 1. 6 Equiaxed grains found in polysilicon sample annealed at 1375°C for 6 hours.[6] No secondary or abnormal grain growth is observed even after 24 hours of annealing.

1.4 Overview

This thesis makes use of various methods in order to characterize the polysilicon and aerosol products from a FBR. This material is compared to other similar silicon grown in other forms as thin films and bulk polysilicon in order to establish similarities and differences in growth and handling. Chapter 2 will discuss the various characterization methods used to identify the material.

Chapter 3 is the general characterization of the granular material. Macro and microstructures are identified and compared to other silicon materials. Heat treatments are applied to alter the original microstructures and properties that can be applied to new post-processing methods.

Chapter 4 describes the homogeneously nucleated particles that are a byproduct of the FBR. These particles are hydrogenated amorphous particles on the nm scale. This chapter describes the effect of heat treatment on the structure of the material and discusses the contribution to the overall growth of the polysilicon granules.

Chapter 5 offers conclusions and summations that discuss the possible implications of the results.

1.5 References

[1] Coso G, Canizo C, Luque A. Chemical vapor deposition model of polysilicon in a trichlorosilane and hydrogen system J Electrochem Soc. **155** (2008) D485

[2] Borodulya VA, Vinogradov LM, Rabinovich OS, Akulich AV. Theoretical analysis and modeling of the obtaining of polycrystalline silicon in a fluidized-bed reactor. J. Eng. Phys. Thermophys. **78** (2005) 47

[3] Nakhodkin NG, Rodionova TV. The mechanism of secondary grain growth in polysilicon films. J Cryst Growth **171** (1997) 50

[4] Thomson CV. Secondary grain growth of thin films in semiconductors: Theoretical aspects. J App Phys **58** (1985) 763

[5] Garrison SM, Cammarata SR, Thompson CV. Surface-energy-driven grain growth during rapid thermal annealing (<10 s) of thin silicon films. J App. Phys **61** (1987) 1652

[6] Fancher RW, Watkins CM, Norton MG, Bahr DF, Osborne EW. Grain growth and mechanical properties in bulk polycrystalline silicon. J Mater Sci. **36** (2001) 5441

[7] Pina J, Bucala V, Schbib NS, Ege P, Lasa HI. Modeling a silicon CVD spouted bed pilot plant reactor. Int J Chem React Eng **4** (2006) 1

[8] Ceccaroli, Bruno. "Development of materials for solar energy: The silicon case."136th TMS Annual Meeting and Exhibition. Orlando, FL. 25 Feb, 2007.

[9] Tavoulareas, E. Stratos. Fluidized-bed combustion technology. Annu. Rev. Energy Environ. **16** (1991) 25

[10] Ling HW. U.S. Pat. 3,012,861 (1961)

[11] Iya SK, Flagella RN DiPaolo FS. Heterogeneous decomposition of silane in a fixed bed reactor. J. Electrochem Soc. **129** (1982) 1531

[12] Hsu G, Hogle R, Rohatgi N, Morrison A. Fines in fluidized bed silane pyrolysis. J. Electrochem. Soc. **131** (1984) 660

[13] Rohatgi NK, Hsu GC, Lutwack R. ed. Dismukes JP. Materials and new processing technologies for photovoltaics. Pennington: The Electrochemical Society, Softbound Proceedings. 477 (1982)

[14] Caussat B, Hemati M, Couderc JP. Silicon deposition from silane or disilane in a fluidized bed – part II: theoretical analysis and modeling. Chem Eng Sci. **50** (1995) 3625

[15] Slootman F, Parent JC. Homogeneous gas-phase nucleation in silane pyrolysis. J. Aerosol Sci. **25** 1994 15

[16] Onischuck AA, Strunin VP, Ushakova MA, Samoilova RI, Panfilov VN. Analysis of hydrogen and paramagnetic defects in a-Si:H aerosol particles resulting from thermal decomposition of silane. Phys Stat Sol (b) **193** (1996) 25

[17] Eversteijn FC. Gas-phase decomposition of silane in a horizontal epitaxial reactor. Philips Res. Repts. **26** (1971) 134

[18] Onischuk AA, Strunin VP, Ushakova MA, Panfilov VN. Studying of silane thermal decomposition mechanism. Int J Chem Kinet **30** (1998) 99

[19] Onischuk AA, Levykin AI, Strunin VP, Ushakova MA, Samoilova RI, Sabelfeld KK, Panfilov VN. Aerosol formation under heterogeneous/homogeneous thermal decomposition of silane: Experiment and numerical modeling. **31** (2000) 879

[20] Brodie RC, Bahr DF. Fracture of polycrystalline silicon. Mat Sci Eng. **A351** (2003) 166

Chapter Two: Experimental Methods

2.1 Sample Preparation for Optical and Electron Microscopy

Specimens of granular polysilicon ranging from 1mm to 1cm were obtained from multiple vendors; the majority of the material was supplied by REC Silicon with the addition of a few samples that were manufactured by a separate manufacturer. The samples for optical microscopy were prepared by traditional mechanical grinding and polishing methods. Roughly 10 granules were first inserted into an epoxy mount. Once cured, the mounted specimen was ground with silicon carbide abrasive paper from 240 to 1200 grit to expose the center of the granules. The mounted specimens were then polished using diamond paste from 3.0μm to 0.25μm. The polished samples were etched with an isotropic "HNA" solution composed of 8% hydrofluoric acid, 25% nitric acid, and 67% acetic acid by volume. The solution was applied with a cotton swab. The swab was rolled on top of the sample until it was slightly darkened and the macrostructural features became evident, and then rinsed with deionized water. Optical images were then taken using standard optical microscopy and a digital camera to allow macrostructural features to be measured and analyzed in chapter 3 of this thesis.

Specimens of the granular material used for scanning electron microscopy (SEM; FEI Sirion operated at 20keV) were prepared via fracture. Individual granules were placed in an indented cup-like metal holder for stability. The samples were then sectioned with a Rockwell hardness tester by applying force onto the top of the granule

with a diamond tip until fracture occurred. The samples were then mounted on SEM stubs using conductive copper tape with the flat fracture surface facing upwards. Colloidal silver paint was used to coat the non-fractured portion of the granule as well as a thin perimeter around the edge of the fracture surface to aid in conductivity.

The granules were fractured in order to achieve reproducible images. Earlier samples were prepared in the same manner as the optical microscopy samples; however, certain surface features were lost due to the mechanical grinding and polishing steps. Fractured surfaces always presented a clean and undisturbed view of the macro- and microstructures of the granules.

Samples prepared for the transmission electron microscope (TEM; JEOL 1200 HR operated at 200 keV) required a thinned sample. The first step of sample preparation was pre-thinning using a Gatan Model 623 Disc Grinder (see Figure 2. 1) A single granule with a diameter approximately 3mm in diameter was selected and glued to the center of the metal stub. Low temperature melting wax was used by fracturing a small segment of the wax (approximately 1mm in diameter) and placing it onto the metal stub on a hot plate on medium heat to melt. A single granule was placed onto the melted wax, and the stub was allowed to cool for approximately 10 minutes.

Once the wax cooled, the stub was placed into the handheld polisher with the sample facing outward. The sample was then polished used diamond lapping film and water by performing circular motions around the film. The first side was polished using the following steps: 30µm, 15µm, 6µm, and 1µm to a thickness that is approximately .25mm beyond the thickest portion of the granule. See the appendix for details. The

granule was removed and replaced onto the stub with the granule facing outward. The second side was polished using the same polishing steps as side one to a thickness of 150µm. The sample was then carefully removed from the polisher by melting the wax and sliding the silicon disk off of the stub. The disk was next placed into an acetone bath to remove the residual wax.

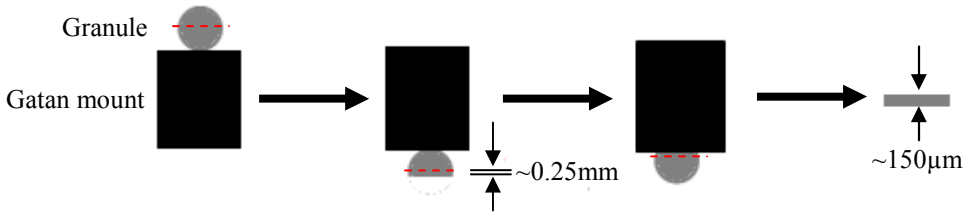

Figure 2. 1 Pre-thinning steps for TEM preparation.

Once the granule has been pre-thinned to an approximate thickness of 150µm, the disk was dimpled using a VCR500i Dimpler (South Bay Technology Inc., San Clemente, CA). See the appendix for details. The sample was first mounted onto a TEM copper grid with epoxy and then onto the center of a glass slide using low temperature melting wax. One side of the silicon was polished in the dimpler using 3 and 1µm diamond slurry for approximately 2 a sample thickness of 0.25µm. The sample was removed and washed with acetone to remove excess wax.

Electron transparency of the silicon was achieved with a VCR ion mill (South Bay Technology Inc., San Clemente, CA) using 5keV argon ions. The sample was placed into the vacuum chamber and evacuated to a pressure of 2.44×10^{-6} torr. Ionized argon gas passing through an acceleration grid is focused onto the sample at very low

angles. The stream of atoms contacts the rotating surface and removes a small portion of silicon atoms from top and bottom of the sample reducing its thickness into a wedge shape with a hole at the center of the sample, as shown schematically in Figure 2. 2. See the appendix for details.

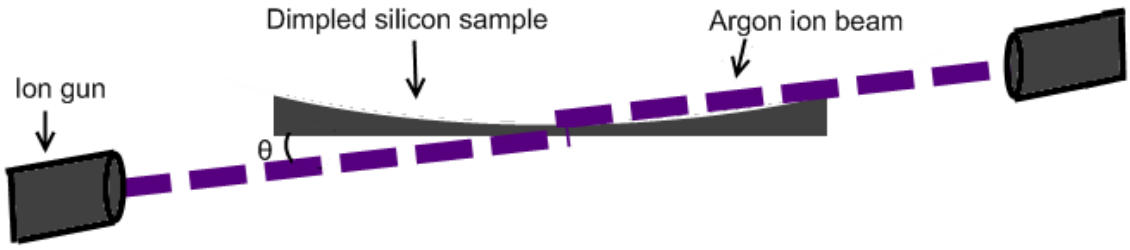

Figure 2. 2 Ion mill setup schematic.

Silicon nanopowers were prepared for TEM work by mixing an approximate 1% by volume solution in methanol. A droplet of this solution is placed onto a copper grid coated with Formvar (polyvinyl formal) and carbon.

2.2 Scanning Electron Microscopy (SEM)

The SEM used for this project is an FEI Sirion operated at 20keV, and was used to examine the surface of the bulk samples. Figure 2. 3 is a schematic of the beam and lenses used inside of column of the microscope.

The condenser and objective lenses used in the SEM are composed of electromagnets. Altering the intensity of these lenses in conjunction with the working

distance between the specimen and final lens can change the probe diameter. The scan coils also located in the chamber can shift the beam to create the scanning raster needed to form a picture.

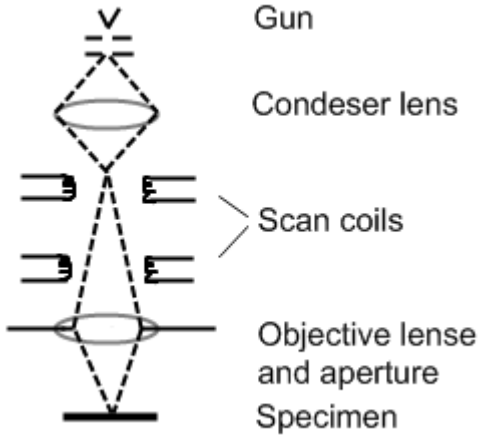

Figure 2. 3 SEM ray diagram schematic.

The image collected digitally is based on the use of secondary electrons that are scattered inelastically from the original source. Secondary electrons are electrons with energy less than 50eV and are detected using a scintillator-photomultiplier system known as the Everhart-Thornley detector. The electrons strike the scintillator (phosphor screen) which then emits light that passes through a light pipe to the photomultiplier. The photomultiplier then converts the light into electron signals that can be transferred to a digital image. In order to direct the secondary electrons to the detector, a metal grid is placed around the phosphor screen with a positive bias voltage. Secondary electrons are ideal for creating an image due to their low depth of penetration. This allows for a high depth a field and an image that is easy to interpret with the human eye.

2.3 Transmission Electron Microscopy (TEM)

The TEMs used in this study are a JOEL 2100 HR operated at 200 keV and a JOEL 1200 EX operated at 100eV, and is constructed similarly to the SEM, however it is not used to examine the surface, but the internal structure of a specimen. Samples used in the TEM are required to be very thin (a few microns) and very small in diameter (approximately 3mm). The column of the TEM consists of multiple condenser and intermediate lenses as well as an objective lens. The condenser lenses and aperture are used to focus the beam and to change the spot size. For imaging, the objective lens is used to focus the specimen on an intermediate plane which can then be amplified with intermediate and projector lenses. In order to see a diffraction pattern, the intermediate lens is focused on the back focal plane. The specimen is inserted in a vacuum chamber and located between the condenser lenses and the objective lens. See Figure 2.4 for details.

The majority of the images obtained from the TEM in this study made use of bright field imaging. The general theory for this method is that the majority of the electrons from the beam will pass through the specimen; however areas that have a higher density, thicker section, or have different orientations and defects will scatter more strongly. As a result, these areas appear darker in the final image. This result was particularly useful in this study in order to observe the highly defective structure of the crystalline silicon. Images acquired from the TEM were digitally acquired. Diffraction patterns were also acquired by focusing the image on the back focal plane in order to

observe the pattern created by the scattered electrons. An obvious pattern indicated a crystalline structure while hazy rings were indicative of an amorphous structure.

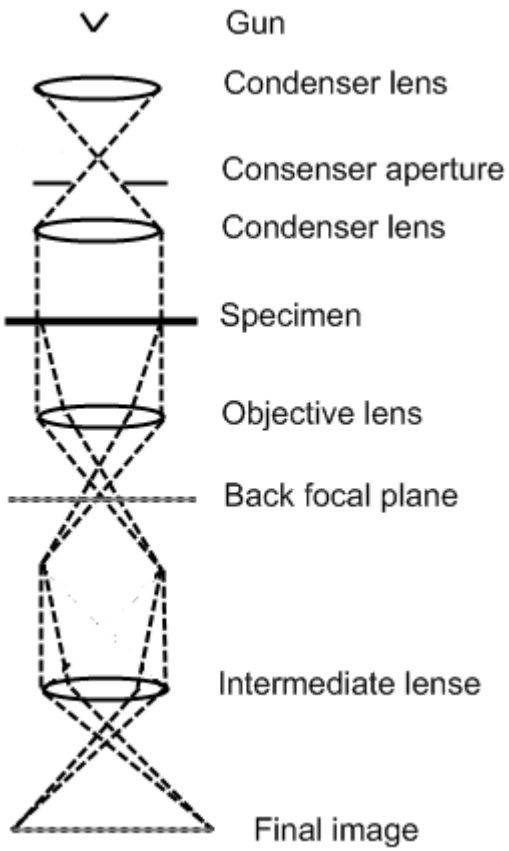

Figure 2. 4 TEM ray diagram focused on the image.

2.4 Fourier Transform Infrared (FTIR) Spectrometry

Chemical bond information for the granular and nanopowder material was obtained from a Fourier transform infrared spectrometer (FTIR). The FTIR is based on the Michelson interferometer which is composed of two mirrors, one fixed and the other moving, and a beam splitter. As seen in Figure 2. 5, a source emits light directed at the

splitter situated at 45° to each of the components. The partially reflective surface creates two beams of light that are aimed at each of the mirrors. The beam is then recombined at the splitter after reflection.[1] Due to the path difference of the moving mirror, an interference pattern is generated. The detector monitors the final beam intensity after it passes through the sample and records it as a function of difference in path. The sample adsorbs certain spectral components of the beam, which becomes representative of sample. The resulting output is referred to as the interferogram, and is the basis for the IR spectra by taking the Fourier transform of the values.[2,3]

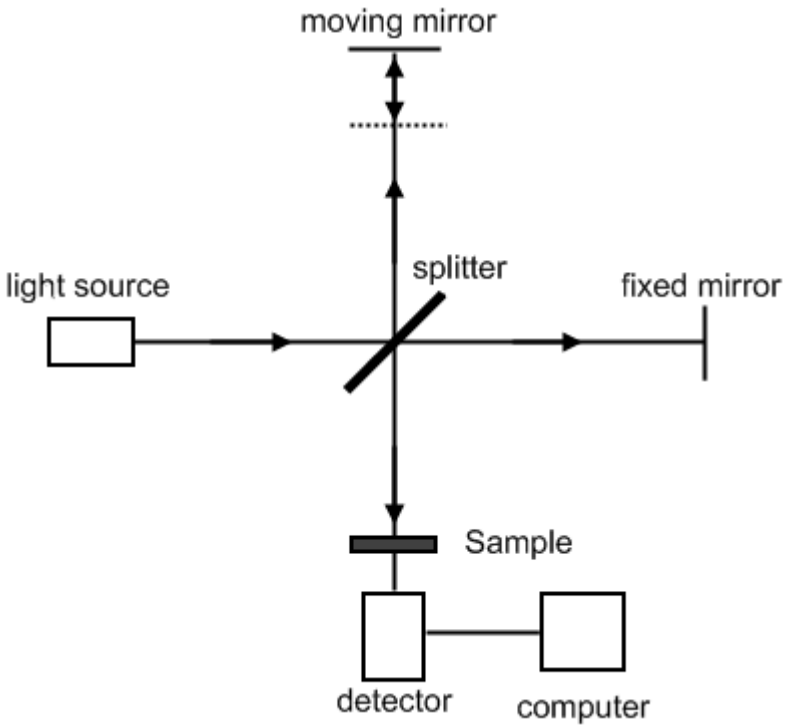

Figure 2. 5 FTIR schematic.

To better understand the FTIR, certain portions of the mathematical manipulations of the spectral data can be explained. The mathematical treatment of the data is first based on the power series expansion of the sine and cosine terms

$$f(x) = a_0 + \sum_{n=1}^{\infty} \left(a_n \cos \frac{n\pi x}{L} + b_n \sin \frac{n\pi x}{L} \right) \quad (1)$$

where

$$a_n = \frac{1}{c} \int_{-c}^{c} f(x) cos \frac{n\pi x}{c} dx \quad (2)$$

and

$$b_n = \frac{1}{c} \int_{-c}^{c} f(x) sin \frac{n\pi x}{c} dx \quad (3)$$

Where a_n and b_n are coefficient's of the n^{th} term and c and L are constants.

However, if terms that are not periodic or are only periodic on an (-∞, ∞) interval are considered a Fourier pair is formed. The first of the pair, the spectra, represents the signal intensity, I, as a function the wavelength, λ. The second of the pair is the interferogram and is the signal as a function of the path difference, D. The resulting graph is a cosine function. Figure 2. 6 A represents a monochromatic source, while Figure 2. 6 B shows a polychromatic or white radiation source. The cosine representation of the second Fourier pair has changed due to the addition of an infinite number of cosine functions at different amplitudes and wavelengths.[3]

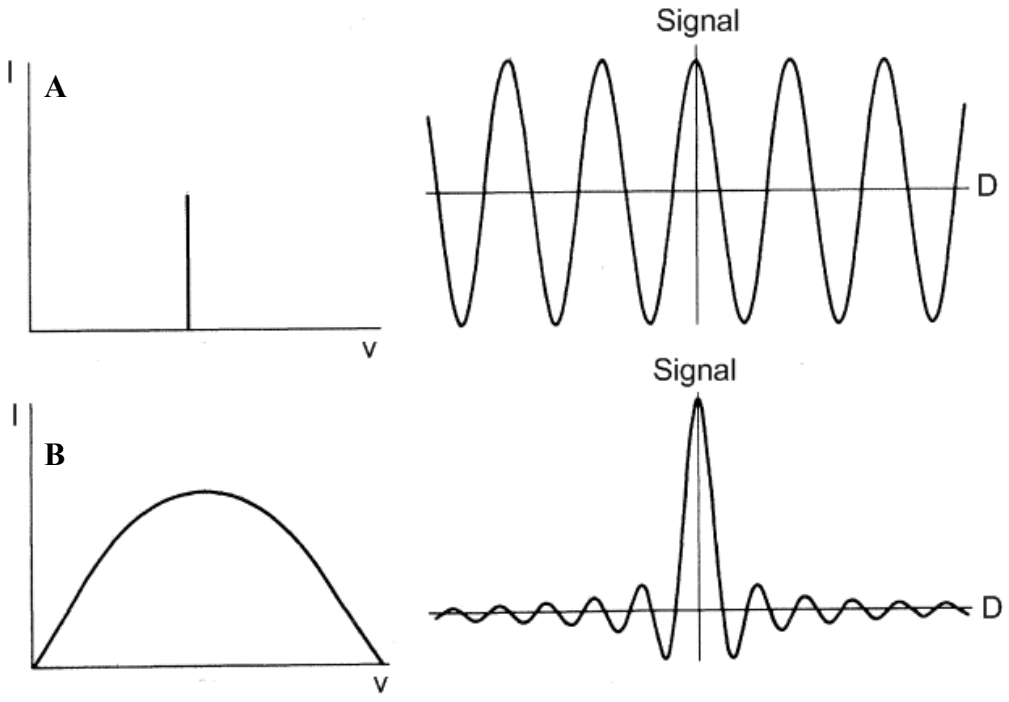

Figure 2. 6 Spectra and interferogram for A) monochromatic radiation and B)polychromatic radiation.[3]

Although the spectra data technically depends on the path difference limits from $(-\infty, \infty)$, this distance is not physically possible; therefore it become necessary to apply the analogy of the partial sums of the Fourier series representation of the square-wave function. In the square-wave function, as the number of terms are increased, the closer the approximation represents the actual function. This approximation is analogous to the FTIR in which the larger the path difference, the more terms are included, and the closer the representation of the actual data.

Resolution of the FTIR depends on the mirror distance from D=0, L, where L=D/2. The mirror must move enough to cause the beam to come out of phase; hence

$$\Delta v = \frac{1}{2D} \quad (4)$$

2.5 FTIR spectrometer sample preparation and peak identification

A BOMEM DA8 FTIR spectrometer was used for this work. The obtainable resolution for this machine is 0.02cm^{-1}. Sample preparation includes the formation of a 5% by mass Si powder in KBr powder solid pellet with a commercial hand press. The powder was inserted into a 7 mm die, and pressure was applied to a dial controlled handle. The addition of KBr was mixed using a mortar and pestle to act as in IR transparent binding agent for the Si powder.

After the sample has been inserted into the die, it is loaded into the sample compartment. The compartment is then evacuated to reduce the absorption of CO_2 and H_2O from the air. The data acquisition is performed by BOMEM PCDA software.

As the light passes through the sample material, the spectral components absorbed give the resulting data a unique spectral signature due to certain wavelengths that are absorbed by specific bonds between atoms. These specific locations are identified by peaks in the resulting spectral data and can be measured to find the relative peak intensities by integrating under the peak's curve. The larger the intensity, the more bonds are present in the material.

Peaks associated with Si range from wavenumbers in the 600 to 2300cm^{-1} spectrum, [4-7] however due to water contamination, the peaks that this study is interested in lie between 2000 and 2300 cm^{-1}. Figure 2. 7 is an example two single peaks and one

doublet peak associated with H and Si observed in this study in an as received batch of Si nano-powder. Literature research reveals that these peaks are documented in other cases, however not all are present in the same source as seen in Figure 2.8.

The first peak, located near 2000cm^{-1}, is associated with the vibration of silicon monohydride (SiH) bond.[7] The doublet peak contributing to the 2100cm^{-1} peak has been associated with the silicon monohydride[4-7] and silicon dihydride (SiH_2)[4] stretching vibrations. The last peak located near 2250cm^{-1} has been documented to be associated with vibrations of SiH bonds backbonded to an O_3 molecule.[5,6]

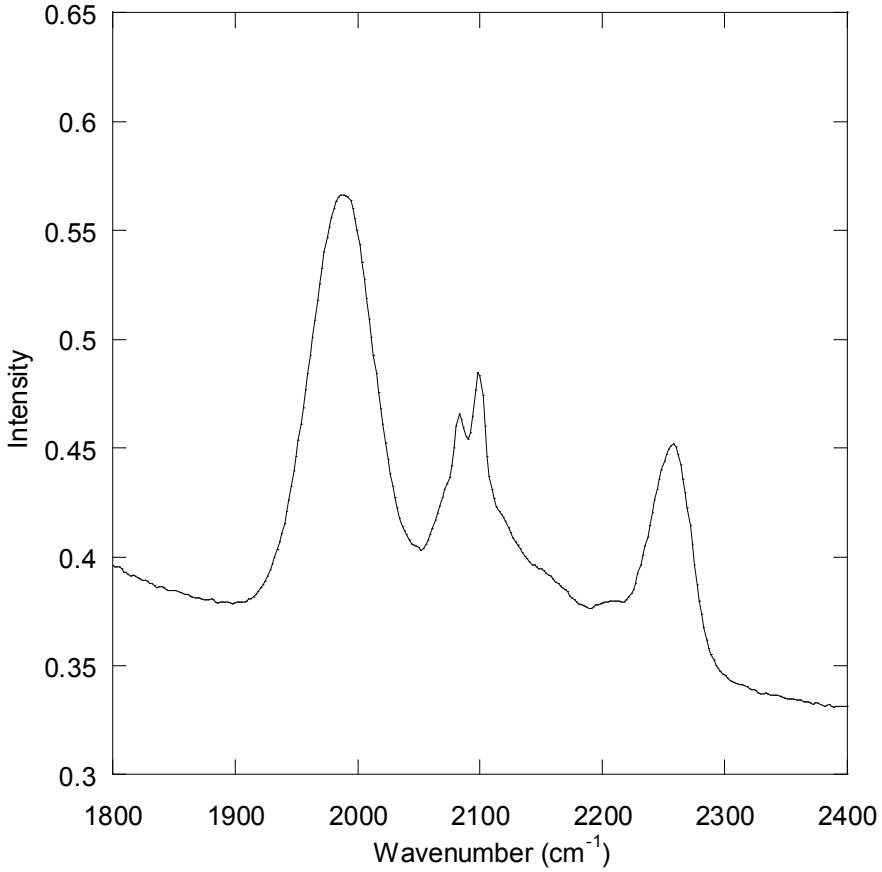

Figure 2. 7 FTIR Si signature spectra.

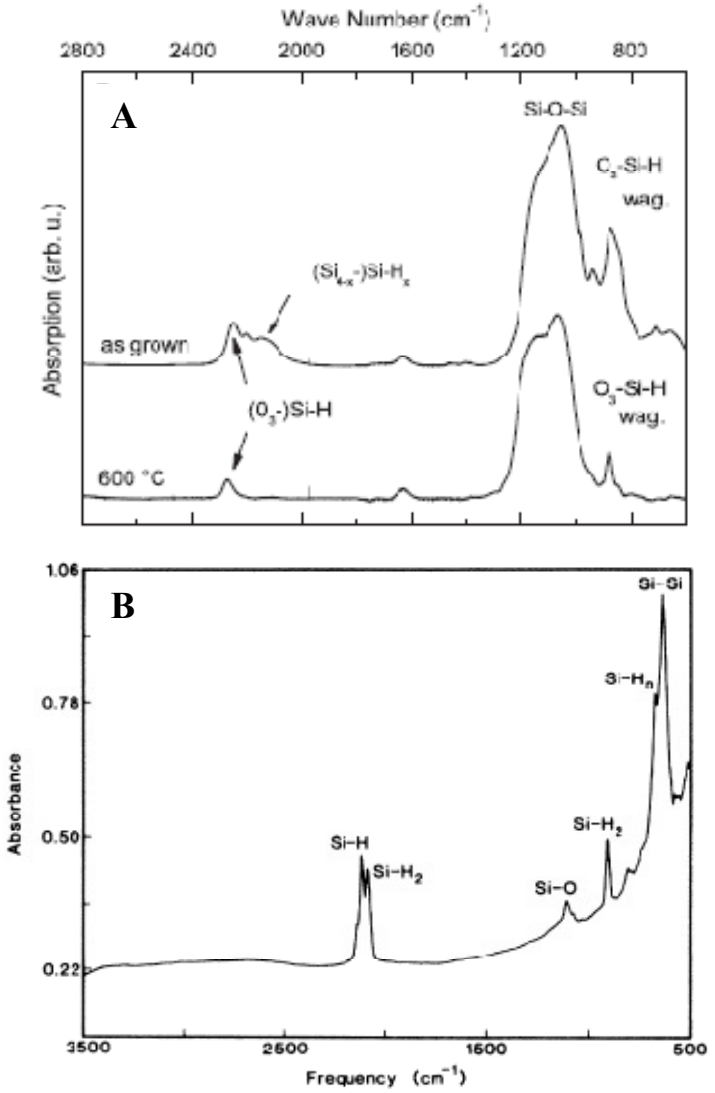

Figure 2. 8 FTIR spectra from literature from A) Stegner[6] and B) Gupta[4]. Elements of spectra are similar in each source, but not complexly the same.

2.6 X-Ray Diffraction (XRD)

X-ray diffraction was performed with a Siemens D-500 X-ray Diffractometer. Granular material was prepared by crushing the material by use of a mortar and pestle in

order to use powder diffraction. Once a fine powder was achieved, it was place on a glass slide with methanol and smoothed to form a flat surface. Data acquisition was performed with MDI Data Scan at a start 2θ value of 20° and an end value of 80°, the step angle was 0.05° and dwell was set at 2.0 sec. The XRD instrument is composed of a Cu Kα X-ray source and a detector on a circular track that is centered around the sample. Data acquired from this study was based on diffraction of crystalline material and the use of Bragg's law:[8]

$$n\lambda = 2d \sin\theta \tag{4}$$

Bragg's law relates the wavelength and the lattice spacing of the crystalline materials. Figure 2. 9 illustrates the incident wave encountering and diffracting off of the lattice planes. Due to the ability to index lattice spacing with this method, Bragg's law is extremely important for determining crystal structures.

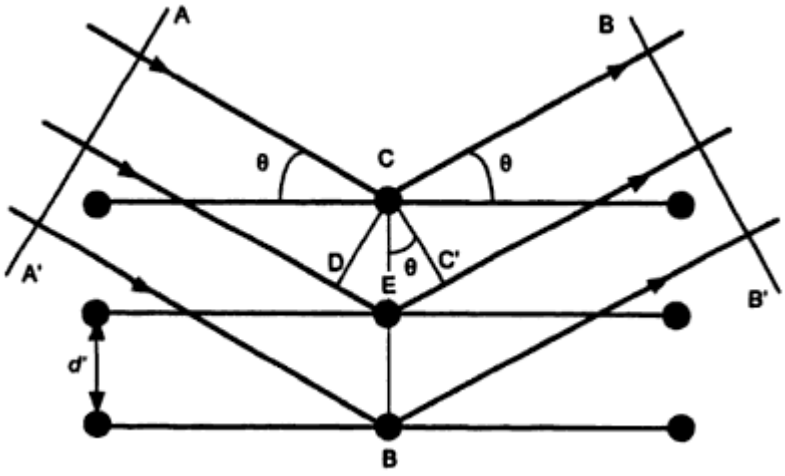

Figure 2. 9 X-Rays encountering and diffracting from a crystalline lattice.[8]

Output data consists of a series of identifying peaks at specific 2θ locations for a material. Because the wavelength and lattice spacing are constant, the data generated relies on detecting more X-rays at angles that satisfy Bragg's law. In a perfectly single crystalline or large grained material, the peaks will be very narrow and centered over the angle that perfectly satisfies Bragg's law. As the grains become smaller, the diffraction of the X-rays becomes imperfect at grain boundaries and at distortions in the lattice, and the peak over the angle widens. It becomes necessary then to measure the full width at half of the maximum intensity (FWHM) of these peaks to get an accurate depiction of their size. The change in the FWHM between a single crystal and a specimen with small grains can be used to determine the size of the grains. The Hall-Williamson equation[9]

$$B\cos\theta = \frac{k\lambda}{D} + \eta\sin\theta \tag{5}$$

is used in this study to determine the grain size, where B is the peak width difference, k is a constant (~1), λ is the X-ray wavelength, η is the strain, and D is the average grain size.

2.7 References

[1] John F. Ready. Industrial Applications of Lasers. San Diego: Academic Press, 1997

[2] Hlaing Oo, Win Maw. Infrared Spectroscopy of Zinc Oxide and Magnesium Nanostructures. Diss. Washington State University, 2007.

[3] Bates JB. Fourier transform infrared spectroscopy. Science **191** (1976) 31

[4] Gupta T, Colvin VL, George SM. Hydrogen desorption kinetics from monohydride and dihydride species on silicon sufraces.Physical Review B. **37** (1988) 8234

[5] Stefanov BB, Gurevich AB, Weldon MK, Raghavachari K, Chabal YJ. Silicon Epoxide: unexpected intermediate during silicon oxide formation. Phy. Rev. Letter. **81** (1998) 3908

[6] Stegner AR, Pereira RN, Klein K, Wiggers H, Brandt MS, Stutzmann M. Phosphorus doping of Si nanocrystals: Interface defects and charge compensation. Physica B. **401-402** (2007) 541

[7] Onishchuck AA, Levykin AI. Etc. Aerosol Formation under heterogeneous/homogeneous thermal decomposition of silane: experiment and numerical modeling. J. Aerosol Sci. **31** (2000) 879

[8] C. Suryanarayana, M. Grant Norton. X-Ray Diffraction: A Practical Approach. New York: Plenum Press, 1998

[9] Williams GK, Hall WH. X-ray line broadening from filed aluminum and wolfram. Acta Mater. **1** (1953) 22

Chapter Three: Characterization of Granular silicon Grown via Fluidized Bed Reactors

3.1 Introduction

Polycrystalline silicon is the base material used in the production of single crystal silicon for the semiconductor industry and for the rapidly growing photovoltaic (PV) market. The most common source of polycrystalline silicon (polysilicon), as previously discussed, has traditionally been via chemical vapor deposition (CVD) in Siemens-style reactors,[1] in which silane or trichlorosilane is decomposed on the surface of a seed rod in which the surface temperature is controlled by internal resistance heating of the rod. This technique requires expensive capital equipment, may have high operating costs, often produces low silicon yield (up to 60% from the gas in theory, but only 15-30% in practice), and generates the release of highly corrosive hydrogen chloride, further adding to capital expense.[1]

The rapid increase in demand for silicon for PV use has surpassed the demand in the microelectronic industry in recent years and has stimulated the need for a more cost effective method to produce larger quantities of polysilicon.[2,3] One method that is gaining popularity is the fluidized bed reactor (FBR) that produces silicon in the form of granules instead of the traditional rods. The purity level of the granular material may be lower than that grown by the Siemens' process, but this appears to be acceptable for the PV market.

As previously discussed in chapter 1, fluidized bed reactors produce granular silicon by pyrolytic decomposition of silane-containing gases on to silicon seed particles in a hydrogen fluidized environment. An important and significant aspect of the FBR is the lower temperature range that is used to produce silicon. Gas decomposition can be achieved at temperatures as low as 600°C, as opposed to temperatures of up to 1200°C that are used in the Siemens process.[4] Once a certain size range is achieved within the reactor, the granules fall to the bottom, where they are collected, without disrupting the growth of the rest of the material. The advantages of the FBR are the lower energy requirements and because it is a continuous process with the ability to recycle the feed gasses very high yields are possible.

Due to the increase in use of FBRs, a better understanding of the granule growth mechanisms and the microstructure and properties of the resulting material is required. These data are available in the literature for bulk polysilicon and thin films,[6-8] but there is no currently available information on the microstructure, properties and subsequent grain growth mechanisms of silicon granules fabricated in the FBR.

In this current chapter, granules grown in the FBR from REC Silicon have been analyzed to determine the structure and morphology of the silicon product. Optical and electron microscopy, X-ray diffraction, and nanoindentation were used to determine grain size, structure, and mechanical properties, respectively. Samples were also annealed at temperatures ranging from 800 to 1100°C to determine the effect of post growth heat treatment on microstructure and mechanical properties of the granules.

3.2 Experimental Procedure

Specimens of granular polysilicon collected from REC Silicon were prepared for optical microscopy by conventional metallographic grinding and polishing. The polished samples were etched with an isotropic "HNA" solution composed of 8% hydrofluoric acid, 25% nitric acid, and 67% acetic acid by volume. Samples were etched with a cotton swab for roughly one minute until the surface darkened slightly and the macrostructure became apparent, and then rinsed with deionized water. Optical images were captured and measurements of the macrostructural features were recorded. Unlike bulk polycrystalline material grown via the Siemens process, the etchant does not reveal the fine sub-μm grain structure; therefore X-ray diffraction was used on powdered granules to determine the average grain size using the Hall-Williamson equation[8]

$$B\cos\theta = \frac{k\lambda}{D} + \eta\sin\theta \tag{6}$$

where B is the peak width difference, k is a constant (~1), λ is the X-ray wavelength, η is the strain, and D is the average grain size.

Samples were prepared for scanning electron microscopy (SEM; FEI Sirion operated at 20keV) by fracturing the samples with a Rockwell hardness tester. Structures, such as internal pores were strongly influenced by the polishing process; the fractured surface produced more reproducible images of the pores and the peripheral fine grain structure. Samples were prepared for transmission electron microscopy (TEM; JEOL 1200 HR operated at 200 keV) by mechanical diamond polishing to 0.25 μm and dimpling using a VCR 500i Dimpler. Electron transparency was achieved with a VCR ion mill using 5 keV argon ions. Annealing of the samples was carried out in an open

platinum crucible that was heated to 800°C at 8°C/min and then at a rate of 4°C/min to the final annealing temperatures of 800°C to 1100°C. The annealed samples were held at the peak temperature for 6 hours and then furnace cooled.

The mechanical properties were measured using a Hysitron Triboscope nanoindentation system in conjunction with a Park Autoprobe CP scanning probe microscope. Indentations were carried out on granular material ground with SiC to a 600 grit finish, and polished to a 0.25 μm finish using diamond polishing compound. The polished surface was imaged using the scanning probe system, and pore-free regions of the surface were selected for indentation. Indentations were carried out using a fixed 10 s loading, 10 s hold, and 10 s unload, with a 5s hold for drift correction, to maximum loads between 4000 and 9500 mN. The unloading slope was analyzed using the Oliver and Pharr method[9] to determine the elastic modulus and hardness of the material. In addition to the granular material, (001) oriented single crystals of silicon were indented for comparison purposes under the same loading conditions.

3.3 Results and Discussion

3.3.1 Microstructure and porosity in as-grown material

Macroscopically, the sectioned granules show a series of concentric rings (Figure 3. 1). The ring structure is evident because of porosity differences within the granule; this suggests multiple growth layers. The darker contrast rings in figure 1 represent regions of higher porosity, while dark radial stripes are due to cracks that were either formed during growth or sample preparation.

Figure 3. 2 and 3.3 are a low magnification and mid magnification SEM image in which the pores forming the rings are very obvious. A more detailed examination of many of these images reveals that each layer has approximately the same radial distance and that all specimens examined share comparable ring dimensions (Figure 3.4 A). There is a roughly linear relationship between the spacing and the position of the rings. Similarly, the number of rings and the total particle diameter as shown in Figure 3.4 B suggests that the radial growth rate is constant. In addition to the radial distance analysis, is an example of a granule that broke while in the reactor and continued to grow. It is assumed that subsequent growth occurred at the same rate. The similar layer thicknesses indicates that the deposition process is limited by surface area and not by the quantity of silicon containing gas or time spent during growth of an individual ring; either of these processes would lead to thinner rings around the exterior of the granule to create similar volumes of material per growth period. Samples grown under a wide range of processing conditions exhibited the porous structures, suggesting these morphological structures are likely suggestive of granular silicon grown via the FBR method. As particulate matter in an FBR will cycle through the height of the column during growth, we suspect these rings containing a relatively high density of voids are linked to the cyclic nature of the growth. However, we do not have direct evidence of where in the growth cycle these voids form, as there is an unmeasured temperature and concentration gradient in the growth chamber.

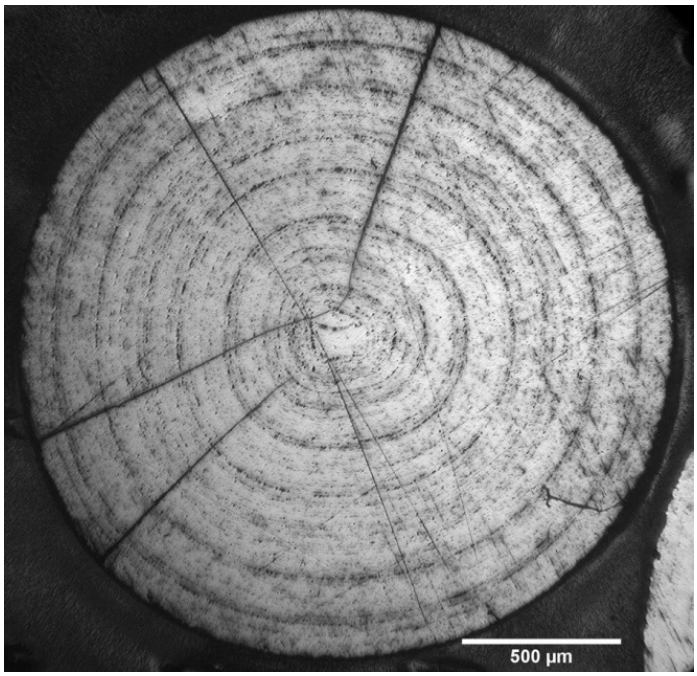

Figure 3. 1 Optical micrograph of sectioned bead.

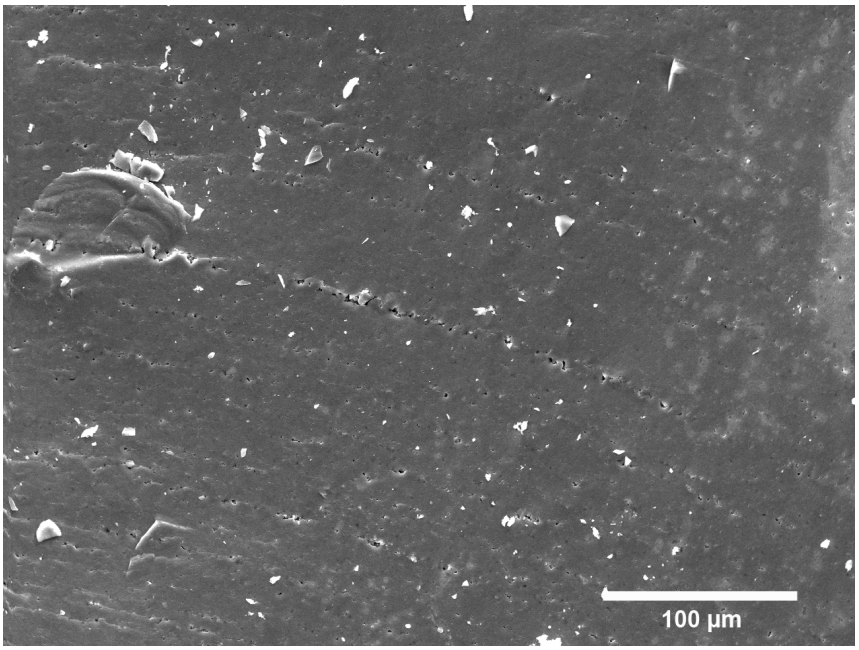

Figure 3. 2 SEM micrograph of porous rings.

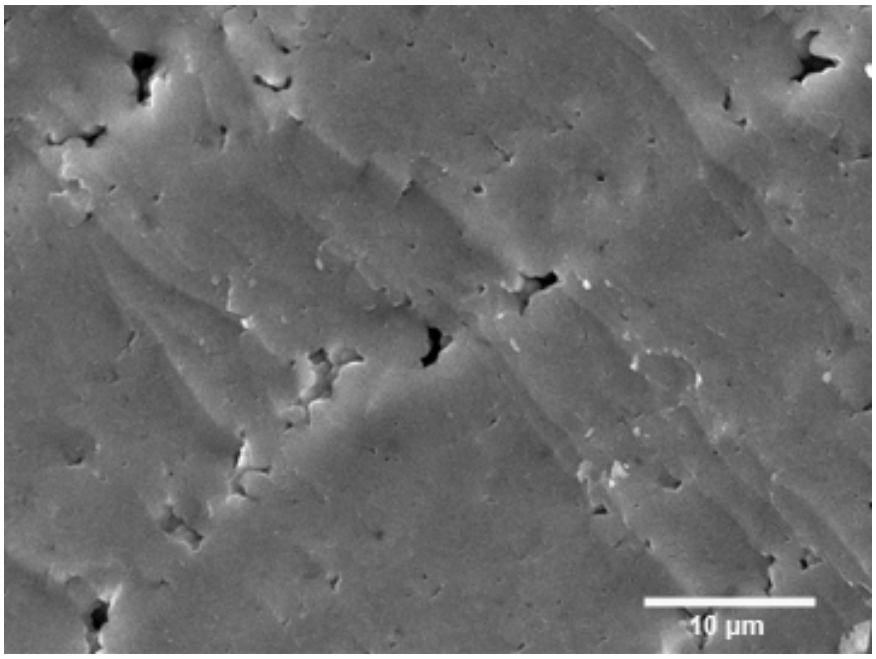

Figure 3. 3 SEM mid-range micrograph of porous rings.

The detail of the pore structure within the rings exhibiting the darker contrast was examined using SEM. In the as-received state, the pores are bounded by spherical particles approximately 0.5 to 1µm in diameter, as seen in Figure 3. 6 A. At higher magnification, Figure 3. 6 B shows that the spheres are textured on the nano level. Figure 3.7 is an image from granular material grown from a second industry source showing a similar pore. Examining a second source verifies that these pores are characteristic features in granular silicon grown in a FBR, and not something related solely to the growth conditions used at REC Silicon.

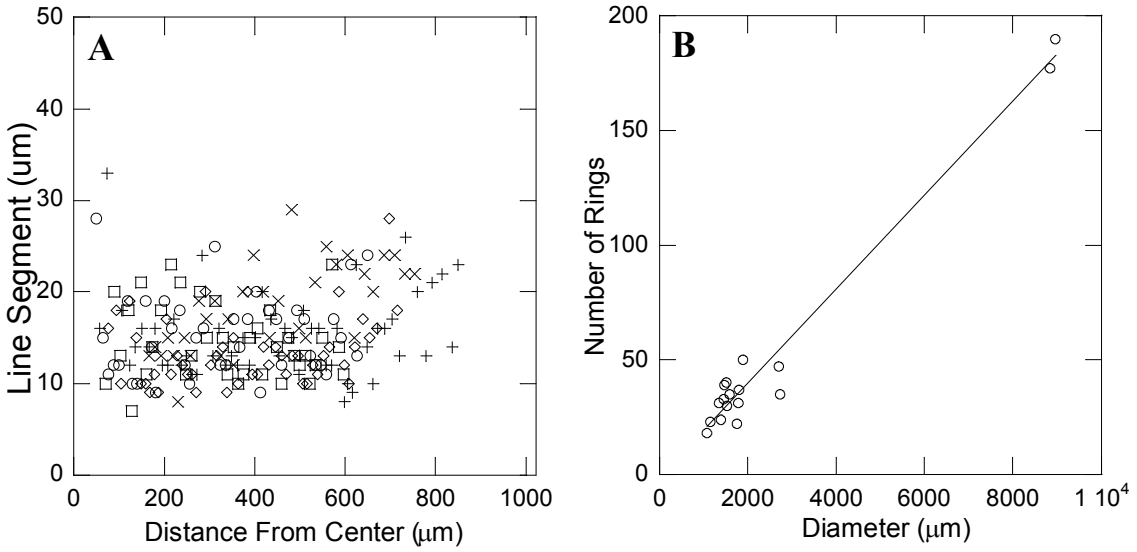

Figure 3. 4 Evidence suggests that the growth rate is constant due to A) Granules displaying similar radial dimensions at all distances from the center and B) a linear trend is evident between the number of rings and the diameter of the granules.

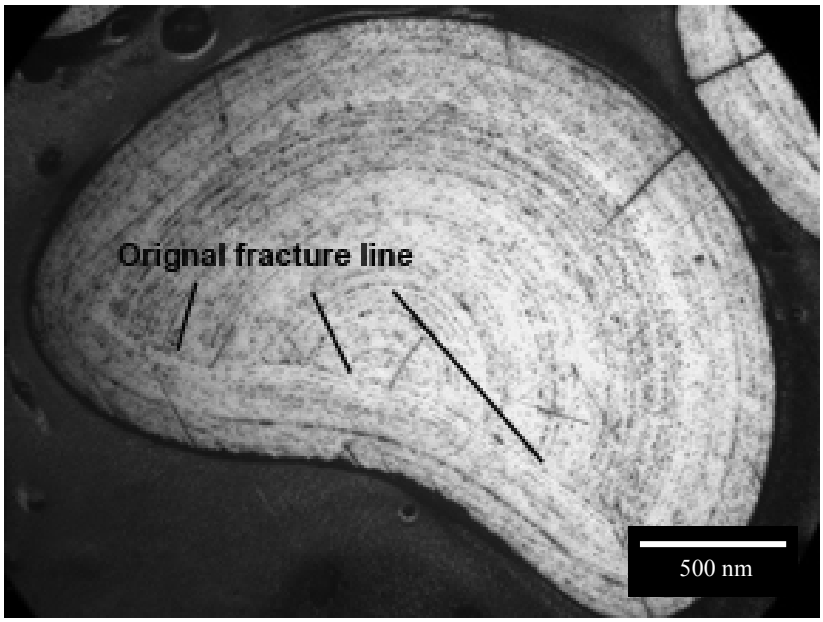

Figure 3. 5 Optical image of fractured granule that continued to grow inside the reactor.

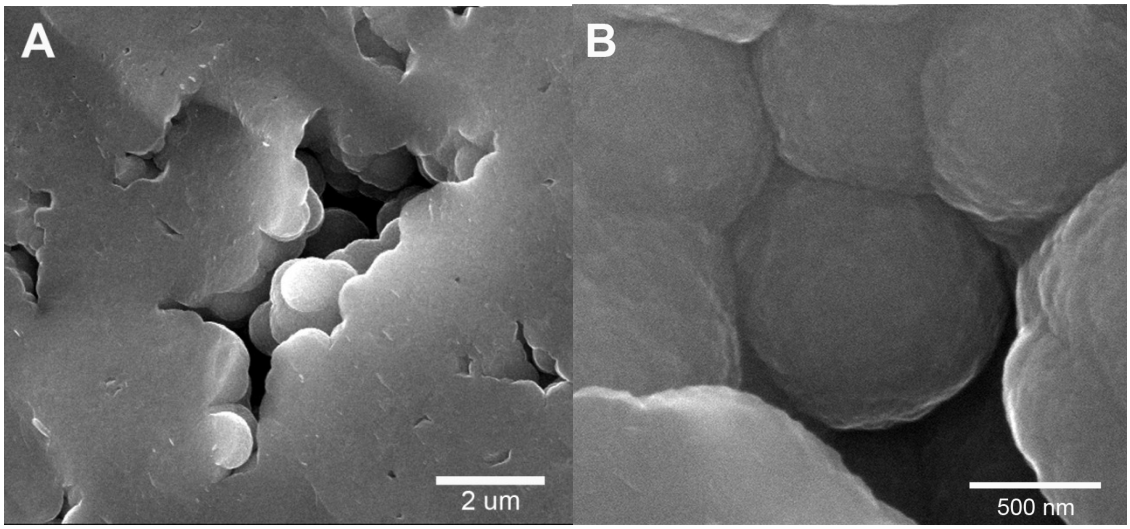

Figure 3. 6 Dark rings are composed of pores approximately 5µm in diameter A) SEM micrograph of pore B) Higher magnification image showing texturing of grains around the pore.

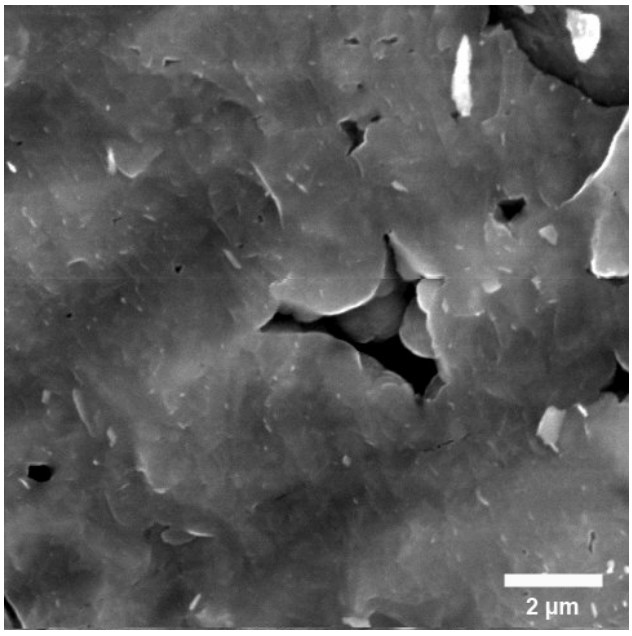

Figure 3. 7 SEM image of pore in second industry source.

3.3.2 Grain size and growth

Grain sizes measured for samples annealed up to 1000°C are shown in Table 3. 1. No significant grain growth is observed until 1000 ºC. Beyond 1000°C, abnormal grain growth leading to a non-Gaussian grain size distribution makes the use of the Hall-Williamson analysis inappropriate for quantifying grain size.

Table 3. 1 Average grain size after annealing at various temperatures for 6 hours.

Annealing Temperature, °C	Average grain size, nm
As Received	30
800	22
900	38
1000	77

Annealing the granules at 1100°C caused an obvious change in the appearance of the pores. The grains around the pores became faceted as illustrated in Figure 3.8A (Non-faceted walls can be seen in Figure 3.8B to compare). This observation suggests that atomic mobility is sufficient to lower the overall surface energy of the grains. Grain growth mechanism changes have also been noted to begin in polysilicon thick films at similar temperatures and are theorized to be a result of a shift of driving force to surface energy anisotropy.[10]

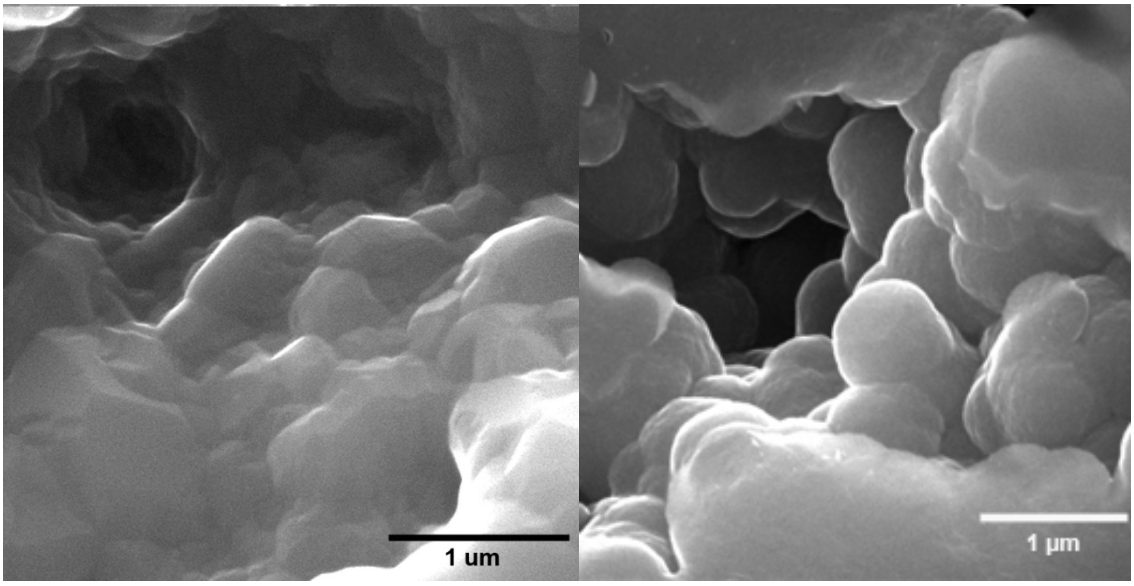

Figure 3. 8 A) Faceted walls of pore in sample annealed at 1100°C for 6 hours. B) Rounded walls of a pore.

Figure 3.9 A and Figure 3.9 B are TEM micrographs that show the grain structure of samples annealed at 1100°C. The images are of fine grained silicon and a large, abnormal grain surrounded by fine grains, respectively. It is noted in Figure 3.9 A that after annealing at 1100°C there are still very fine grains, less than 20 nm in diameter, even though there is an overall increase in grain size as the annealing temperature is increased. The abnormal grains ranged from 200nm to 500nm in diameter. The presence of large grains indicates abnormal grain growth in samples annealed at the higher temperatures used in this study.

It should be noted that both the abnormal grains as well as the primary grains are heavily twinned. Higher magnification imaging in the TEM illustrates the magnitude of

twinning present in the material. Figure 3.10 is an example of the twin sizes that are generally on the nm scale. The grain growth appears to be similar to that seen in polycrystalline thin and thick films grown via CVD and plasma-enhanced CVD; [5] however the driving force is most likely related to grain boundary energy reduction as seen in bulk systems and less dependent on surface energy as would be expected in thin film growth. Secondary grain growth in polysilicon thin films is driven by the surface energy reduction of large columnar grains;[6] however grain growth in thick films that does not depend upon the columnar grain structure has been investigated to produce secondary grain growth by other means[10]. For example, other studies at high temperatures (above 1040°C) and shorter times (approximately 30 minutes), have shown secondary grain growth and attributed it to coalescence due to dislocation climb in grain boundaries. At longer times, grain growth appears to be attributed to surface energy anisotropy[10] and the newly formed abnormal grains continue to grow at a faster rate than the regular sized grains.

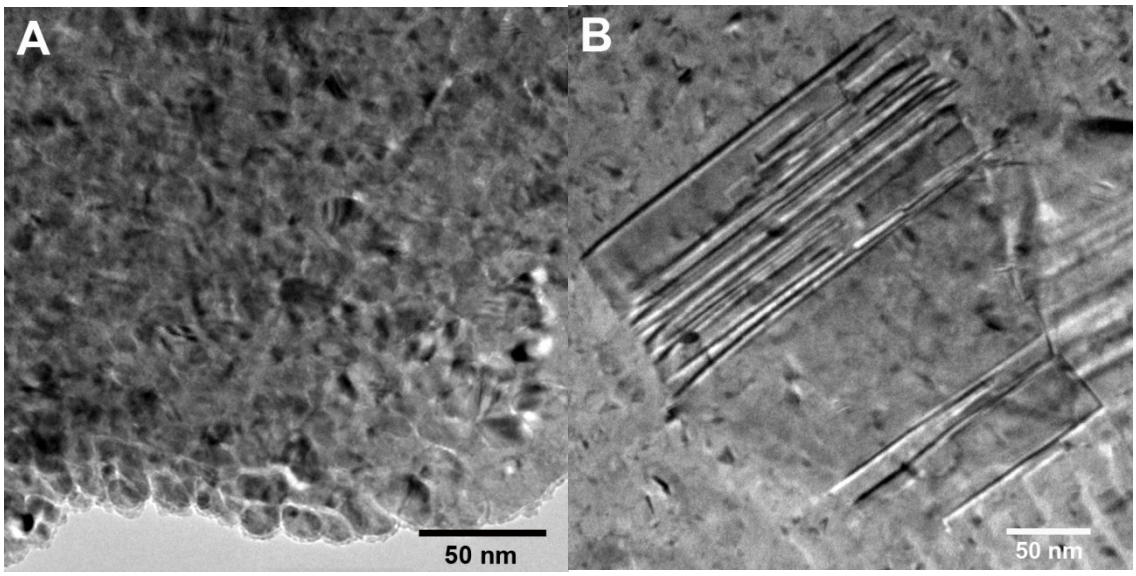

Figure 3. 9 TEM micrograph of A) Grains approximately 30 nm in diameter. B) Abnormal grain growth present in annealed sample at 1100°C.

The activation energy for primary grain growth (where the grain size distribution remains monomodal, in this case at and below 1000 °C) was determined to be 0.80eV using an Arrhenius analysis. This value is consistent with literature values of activation energies for grain growth in larger grained polycrystalline silicon.[6,11]

Bulk polysilicon grown via conventional CVD methods reported in the literature does not exhibit the same type of as-deposited grains or grain growth found in the FBR granules.[6,7] Bulk polysilicon grown via the Siemens process begins as long acicular grains, which become equiaxed after annealing at temperatures above 1100°C for 12-24 hours. Secondary and abnormal grain growth has not been observed in bulk polysilicon

grown via the Siemens process at these temperatures, whereas it appears to occur readily in the granules grown by in the FBR.

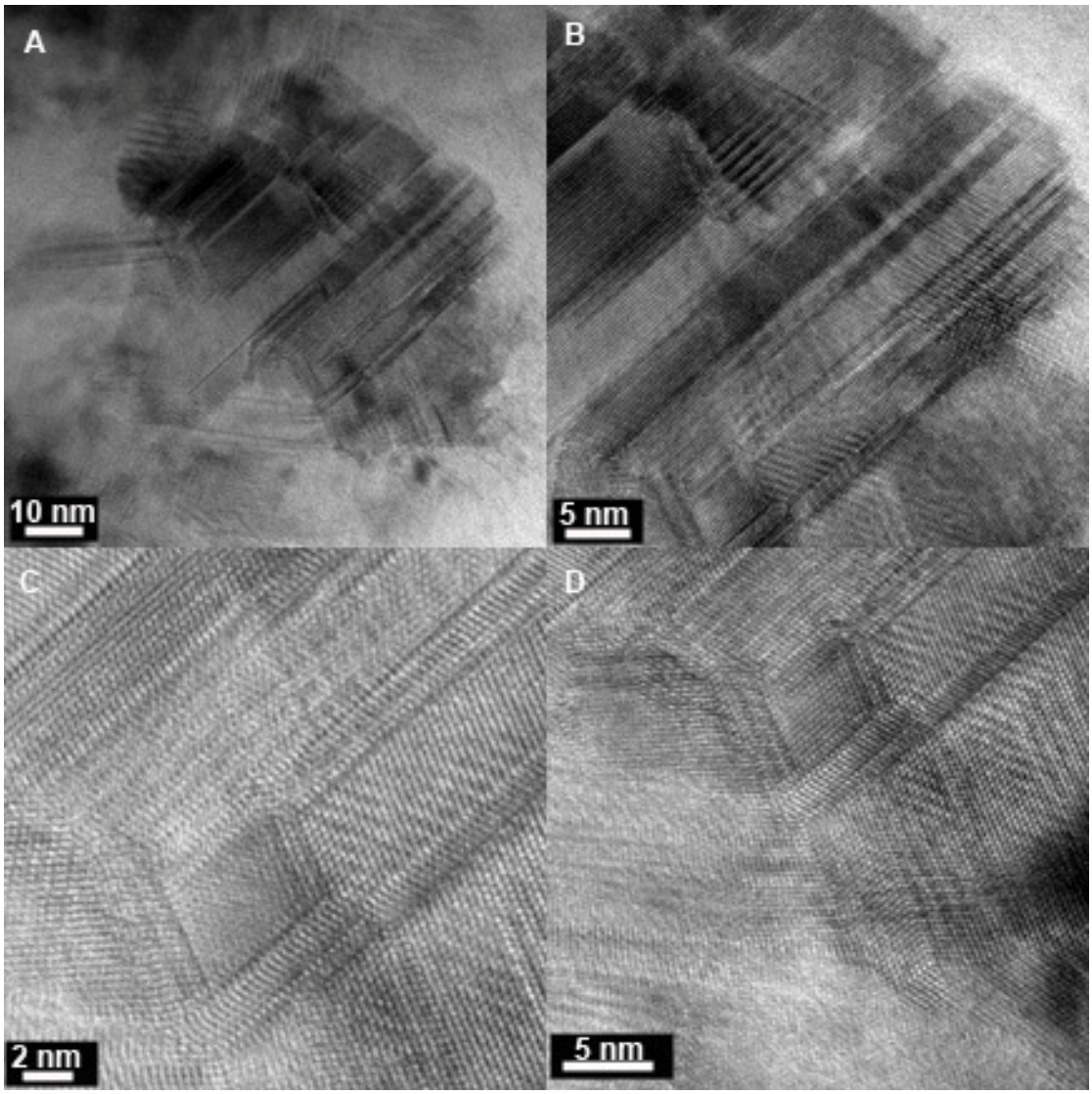

Figure 3. 10 TEM images of a highly twinned grain in an as received sample.

3.3.3 Hardness

Mechanical contact between granular material during handling may lead to fracture, and the fine grain size identified in this paper may lead to more changes in the mechanical behavior in a manner similar to that of other nanocrystalline and ultrafine grained ceramic and semiconductor materials. To inspect the mechanical properties of silicon grown in the FBR independent of the density or morphology of pores the hardness was measured using nanoindentation, as opposed to larger scale Vickers microhardness testing to ensure no fracture events occurred around the indentation. Due to the porous structure of the material, the hardness and elastic modulus are both a function of the contact depth; sampling larger volumes increases the likelihood of pores being present in the elastic stress field around the indentation, which could lead to lower hardness and modulus measurements.[9] Therefore the hardness was measured at contact depths of approximately 100 nm, where the volume of material probed (on the order of a hemisphere 800-1000 nm in diameter) is large enough to be beyond tip rounding effects and is well within the range of the tip area function calibration, but small enough to be relatively insensitive to sub-surface porosity that may be present. In order to ensure no influence of porosity, the calculated hardness value for each of the silicon samples was based on a series of indentations with an average elastic modulus that was comparable to the modulus of a single crystal silicon sample; approximately 147 GPa.

The hardness for two sources of granular material in both the as-received and annealed states is shown in Table 3.2. In addition, Figure 3. 11 illustrates the differences in hardness between the samples in the depth versus load curve. Previously reported

hardness values for bulk and thin film polysilicon are between 10 and 12 GPa.[6,12] In general the hardness of the FBR material is about 10% less than that of single crystal silicon, and annealing does not significantly impact the hardness of the material. This lower hardness is likely attributed to the fine grain structure, which may allow for some grain boundary sliding, a mechanism that would not be available in larger grained material. According to a Mann-Whitney-Wilcoxon statistical test,[13] the sample data do originate from different populations with a p-value of less than 0.0001.

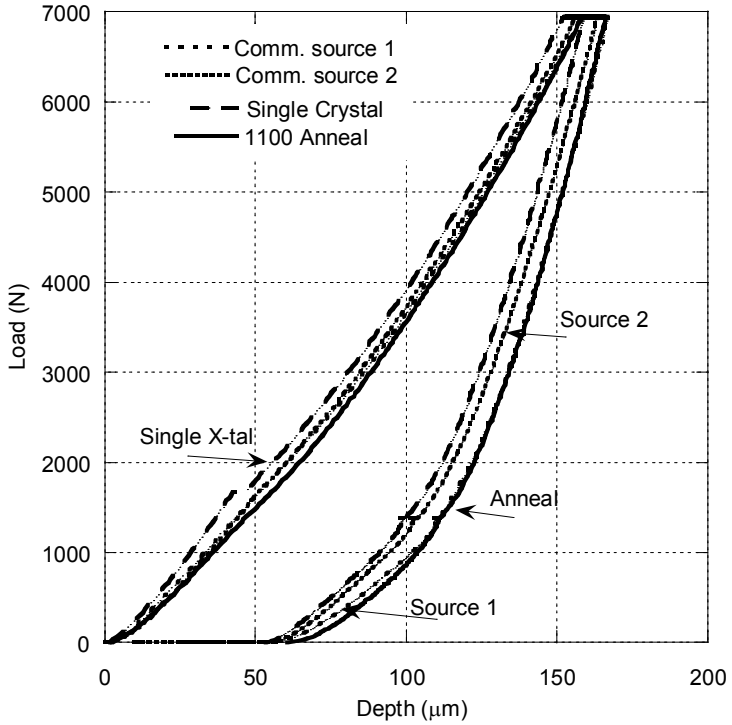

Figure 3. 11 Depth vs. load curve of single crystal silicon and the two granular sources in the annealed and as received state.

Table 3. 2 Silicon modulus and hardness values.

	Elastic Modulus (GPa)	Hardness (GPa)
Single Crystal	157.3	9.6 ± 0.13
REC granules	155.4	8.6 ± 1.13
Commercial source 2	146.8	9.8 ± 0.88
1100°C Anneal	157.7	8.7 ± 0.94

3.4 Conclusions

Silicon granule material grown in FBRs consists of a macrostructure composed of semi-porous material, in which the closed pores are on the order of 5 μm in diameter, separated by segments of relatively pore-free material with thicknesses between 10 and 20 μm. The grain size of the as-grown material is on the order of 30 nm. On the walls of the pores there are spherical nodules with a nanotexture on the order of the grain size inferred by X-ray diffraction. Annealing below 1000 °C appears to follow similar kinetics for grain growth as other polysilicon materials. At an annealing temperature of 1100°C the pore morphology ceases to be spherical and becomes faceted. Also, when the material is annealed at temperatures above 1100°C, abnormal grain growth is observed for annealing times of 6 hours. The as grown granular material is slightly softer than conventionally grown polysilicon; this is most likely due to the very fine grain structure of the material.

3.5 References

[1] Borodulya VA, Vinogradov LM, Rabinovich OS, Akulich AV. Theoretical analysis and modeling of the obtaining of polycrystalline silicon in a fluidized-bed reactor. J of Eng Phys Thermophys. **78** (2005) 47

[2] Caussat B, Hemati M, Couderc JP. Silicon deposition from silane or disilane in a fluidized bed – part II: theoretical analysis and modeling. Chem Eng Sci. **50** (1995) 3625

[3] Coso G, Canizo C, Luque A. Chemical vapor deposition model of polysilicon in a trichlorosilane and hydrogen system J Electrochem Soc. **155** (2008) D485

[4] Pina J, Bucala V, Schbib NS, Ege P, Lasa HI. Modeling a silicon CVD spouted bed pilot plant reactor. Int J Chem React Eng **4** (2006) 1

[5] Thompson CV. Secondary grain growth in thin films of semiconductors: Theoretical aspects J Appl Phys. **58** (1985) 763

[6] Fancher RW, Watkins CM, Norton MG, Bahr DF, Osborne EW. Grain growth and mechanical properties in bulk polycrystalline silicon. J Mater Sci. **36** (2001) 5441

[7] Brodie RC, Bahr DF. Fracture of polycrystalline silicon. Mater Sci Eng. **A351** (2003) 166

[8] Williams GK, Hall WH. X-ray line broadening from filed aluminum and wolfram. Acta Mater. **1** (1953) 22

[9] Pharr GM, Oliver WC, Clarke DR. Hysteresis and discontinuity in the indentation load-displacement behavior of silicon. Scripta Mater. **23** (1989) 1949

[10] Nakhodkin NG, Rodionova TV. The mechanism of secondary grain growth in polysilicon films. J Cryst Growth **171** (1997) 50

[11] Kalainathan S, Dhanasekaran R, Ramasamy P. Kinetics of grain growth in doped polycrystalline silicon thin films. Thin Solid Films **163** (1988) 383

[12] Bhushan B, Li X. Micromechanical and tribological characterization of doped single-crystal silicon and polysilicon films for microelectromechanical systems devices. J Mater Res **1** (1997) 54

[13] Mann HB, Whitney, DR. On a test of whether one of two random variables is stochastically larger than the other. Annals of Mathematical Statistics. **10** (1947) 50

Chapter Four: Homogeneous Nucleation in the Fluidized Bed Reactor

4.1 Introduction

Fluidized bed reactors (FBR) are being utilized to manufacture polycrystalline silicon for the photovoltaic industry due to the energy and time saving capabilities of the process.[1-3] However, hydrogenated amorphous (a-Si:H) and crystalline aerosol particles have been observed in conjunction with the polysilicon material, and are generally considered parasitic to the growth of the desired granules.[4] This material, also known as powder or fines, is found on the reactor walls and loose within the chamber, and is formed from silane thermal decomposition.[5,6] Previously published results report a size distribution of particles between 5 and 100nm for individual particles and up to 10μm for aggregates.[6-8]

During the traditional chemical vapor deposition and FBR process, silicon fines are produced via homogeneous nucleation when a critical silane concentration and temperature condition is reached.[6,8,9] This critical concentration is defined as the concentration of silane gas needed to begin pyrolysis, and is directly related to the type of carrier gas used in the system.[8] The use of hydrogen instead of inert gasses such as argon, helium, and nitrogen will retard the temperature at which pyrolysis will take place. The change in pyrolysis variables has been linked to the fact that one of the products of the silane reaction is hydrogen gas. It has been theorized that a large excess of hydrogen may influence the gas-phase kinetics and decreases the particle precursor material, and increases the temperature at which pyrolysis will begin.[8-10]

Interest in the aerosol particles has led to considerable research into the growth mechanisms of the particles by other researchers.[5,7,11,12] Parameters such as silane conversion rates, hydrogen evolution, and hydrogen bonds have been monitored during growth to gain insight into the mechanisms leading to aerosol particle growth. Monitoring these parameters has led researchers to conclude that the growth of the particles are dependent on both homogeneous nucleation as well as heterogeneous deposition;[6,8,11] however it is apparent that the heterogeneous contribution remains relatively low compared to the homogeneous decomposition portion for these nm scale particles.[7]

The research described in this chapter aims to examine the secondary aerosol product found in the reactor to clarify its contribution, if any, to the overall growth of the polysilicon material used for photovoltaics. It becomes necessary to then to examine its growth characteristics and relationships with dissolved hydrogen in the solid aerosol particles and temperature. In addition to potential growth impact on the primary granular products in an FBR, understanding the structure and how it is affected by annealing temperatures may enhance the particle's use as a raw product for other applications.

4.2 Experimental Procedure

Silicon fines samples used in various characterization techniques were collected from REC Silicon. Details of the removal and collection of this material from the FBR is further explained in other literature sources.[1,6] Sample preparation for transmission

electron microscopy (TEM; JEOL 1200 HR operated at 200 keV) and Fourier Transform Infrared (FTIR) Spectroscopy required various heat treatments to determine its relationship with a controllable variable such as temperature. To avoid interaction between the silicon powder and gasses such as oxygen and hydrogen, the samples were annealed in a vacuum with Zr ribbon acting as a getter for hydrogen and oxygen. The sample, consisting of approximately a cm^3 of fines was placed inside of a quartz tube, evacuated, and sealed by fusing the tube and a cap with a torch. See Figure 4. 1 for details. The samples were then annealed in a box furnace for 6 hours at a rate of 8°/min to the various soak temperatures between 400 and 750°C in the sealed ampoule.

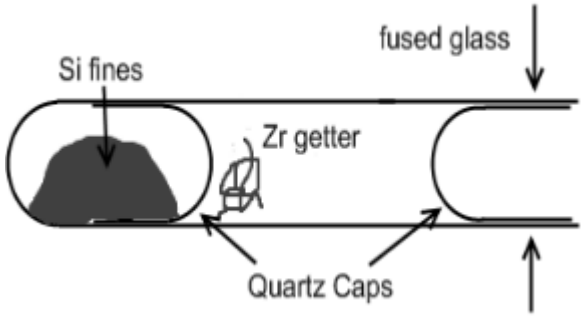

Figure 4. 1 Quartz ampoule in vacuum schematic.

Samples prepared for TEM work were mixed in a 1% by volume solution with methanol. A droplet of this solution was placed on a copper TEM grid coated with Formvar and carbon. The Si powder was prepared for the Fourier Transform Infrared (FTIR) spectrometer (BOMEM DA8) by forming a solid pellet. A 5% by mass mixture of silicon in KBr was placed in a dial controlled hand press. Potassium Bromide was used as an IR transparent binding agent to hold the silicon in a solid pellet form. Further

descriptions on these techniques can be found in chapter two. Annealed fines were tested for hydrogen concentration in a Leco Hydrogen Analyzer by NSL Analytical Services, Inc (Cleveland, OH). Crystallization temperatures were determined by a differential scanning calorimeter (DSC) in Los Alamos National Laboratory (Los Alamos, NM).

4.3 Results and Discussion

Using the FTIR spectrometer, samples annealed at 600, 700, and 750°C were compared to an as received sample and a granular sample to track the changes in bonds associated with hydrogen and silicon. Three silicon-hydrogen peaks are examined in this study; the first peak at 1990cm^{-1} has been determined to be a Si-H bond,[11] the doublet peak[13] in the center at 2100 cm^{-1} is associated with an $(Si\text{-}H_2)_n$ bond [11] as well as an Si-H bond, [14,15] and the third peak at 2270cm^{-1} has been associated with an Si-H molecule back bonded to three oxygen atoms.[14,15] It is apparent from Figure 4. 2 that as the annealing temperature is increased, the intensity of the bonds associated with hydrogen and silicon decrease. It is also evident from this figure that the granular material contains a significant amount of hydrogen. It is theorized that the hydrogen present could be due to hydrogen trapped during granule formation or possibly due to fines agglomeration onto the granule. These theories will be discussed later in detail.

Images obtained from electron microscopy reveal that the majority of the as received sample is amorphous in nature. Statistical analysis of the particle size distribution reveals that the mean and median diameters of these particles are approximately 78 nm (±29.25) as seen in Figure 4.3. This size is in agreement with

previously published literature.[6,8] Figure 4.4 illustrates that as the annealing temperature is increased, a higher percentage of crystalline particles are observed. Also noted in the particles is that there was no partial crystallization in a single sphere. In addition to the changes in the particle structure, a small percentage of necking becomes apparent at temperatures of 700°C and above; however, statistical analysis confirms there is no additional growth in the diameter of the particles.

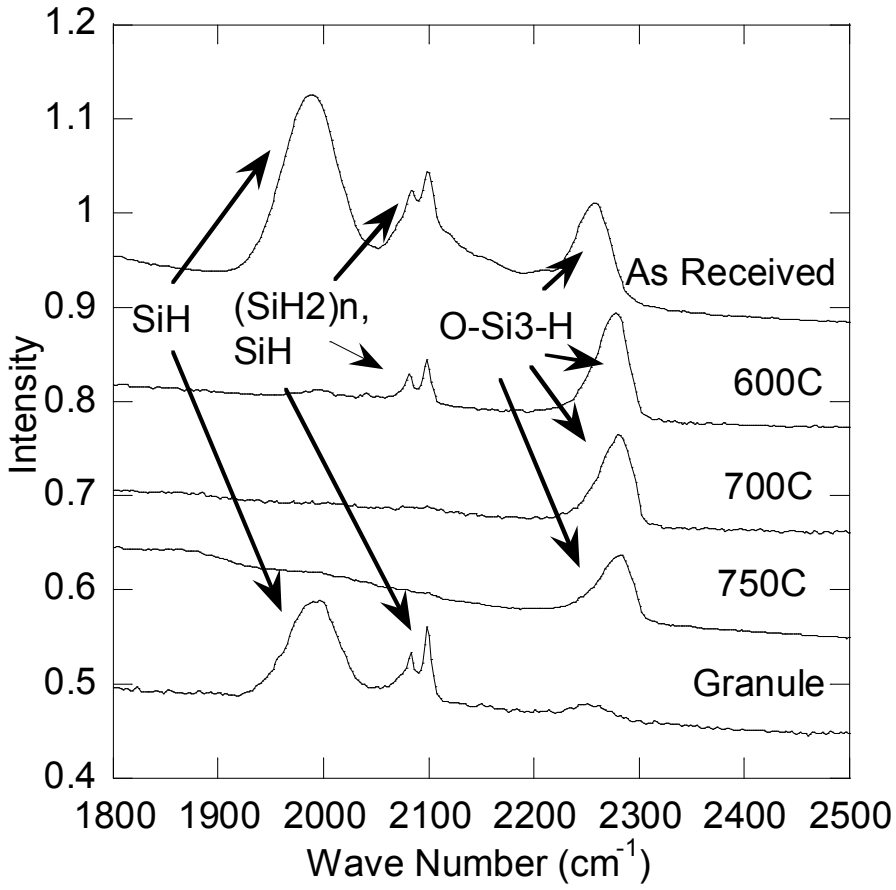

Figure 4. 2 FTIR spectra for as received, annealed, and granular silicon from the FBR.

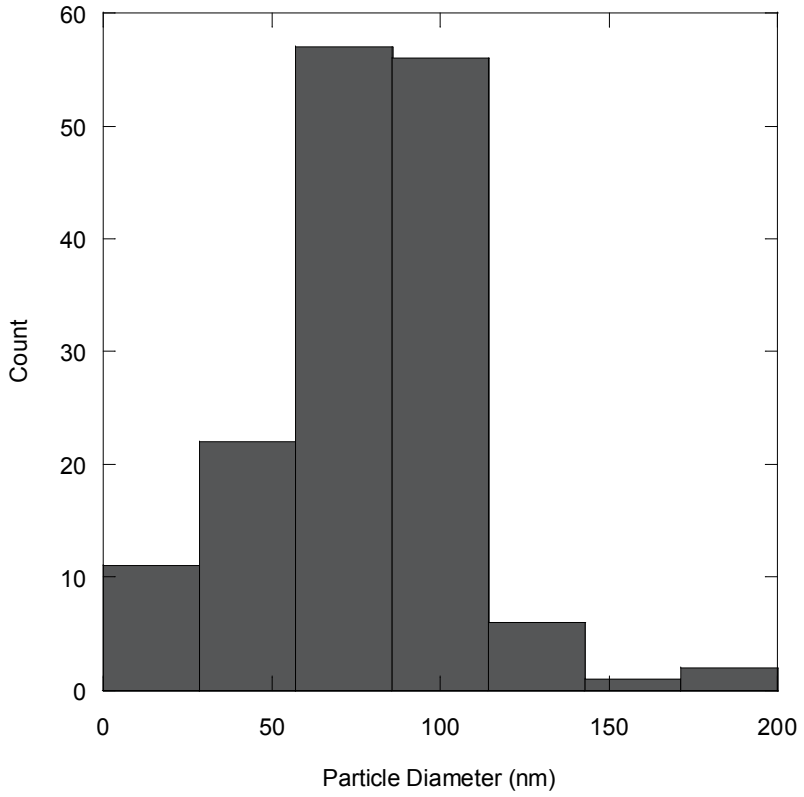

Figure 4. 3 Fines particle size distribution.

Samples annealed at 400, 500, 600, 650, and 700°C were tested for hydrogen content. The results are listed in Table 4.1. In agreement with the FTIR results, as the annealing temperature is increased, the hydrogen content decreases. In addition, calculating the change in mass of the hydrogen illustrates that there is a change in activation energy near 600°C (figure 4.5). The activation energy at the lower temperatures is roughly 5 times greater than the energy required at temperatures above 600°C (0.5 eV and 0.9 eV for high and low temperatures, respectively). Due to a lower activation energy at higher temperatures, it becomes evident that the mechanism for crystallization and hydrogen evolution occurs more easily at temperatures above 600°C,

and the limiting factor is probably related to the surface at lower temperatures. A theory that supports this evidence is related to the difference in bond energies between silicon and hydrogen as well as the volume free energy, ΔG_v, of the particles with different radiuses.

Images obtained from the TEM reveal that as the fines begin to crystallize, smaller particles remain amorphous longer than the larger spheres as the annealing temperature is increased (Figure 4.6). This is validated by Figure 4.7 that illustrates that the lower the hydrogen content, the more volume of material is crystallized with a change in slope near 600°C. The smaller sphere remaining amorphous is explained by relating it to the homogeneous nucleation theory involving ΔG_v:

$$\Delta G = \frac{4}{3}\pi r^3 G_v + 4\pi r^2 \gamma \quad (7)$$

where r is the radius and γ is the surface energy. As the radius of a spherical particle is increased, the free energy is decreased. Thus, the larger the particle, the larger the driving force for crystallization becomes. On the other hand, this driving force must be large enough to overcome the barrier on the surface created by dangling bonds. The energy required to break two Si-H bonds is over 6 eV and is higher than the energy associated with the created of the H_2 molecule (~4 eV). [16] Consequently, the higher surface to volume ratio causes retardation in crystallization for the smaller particles until a higher annealing temperature has been achieved. In other words, there are more dangling bonds per volume of the smaller particles to remove before bulk diffusion can take place. The smaller uncrystallized particles also points to the fact that this transformation is not diffusion limited. In a case where the crystallization and hydrogen

evolution are diffusion limited, one would expect to see the smallest particles to crystallize first. Similar non-diffusion limited mechanisms have been observed in amorphous thin film silicon breakdown.[16]

A differential scanning calorimeter (DSC) scan seen in Figure 4.8 reveals that crystallization occurs at roughly 657°C. This value is in agreement with the TEM and FTIR data that suggests when the material crystallizes.

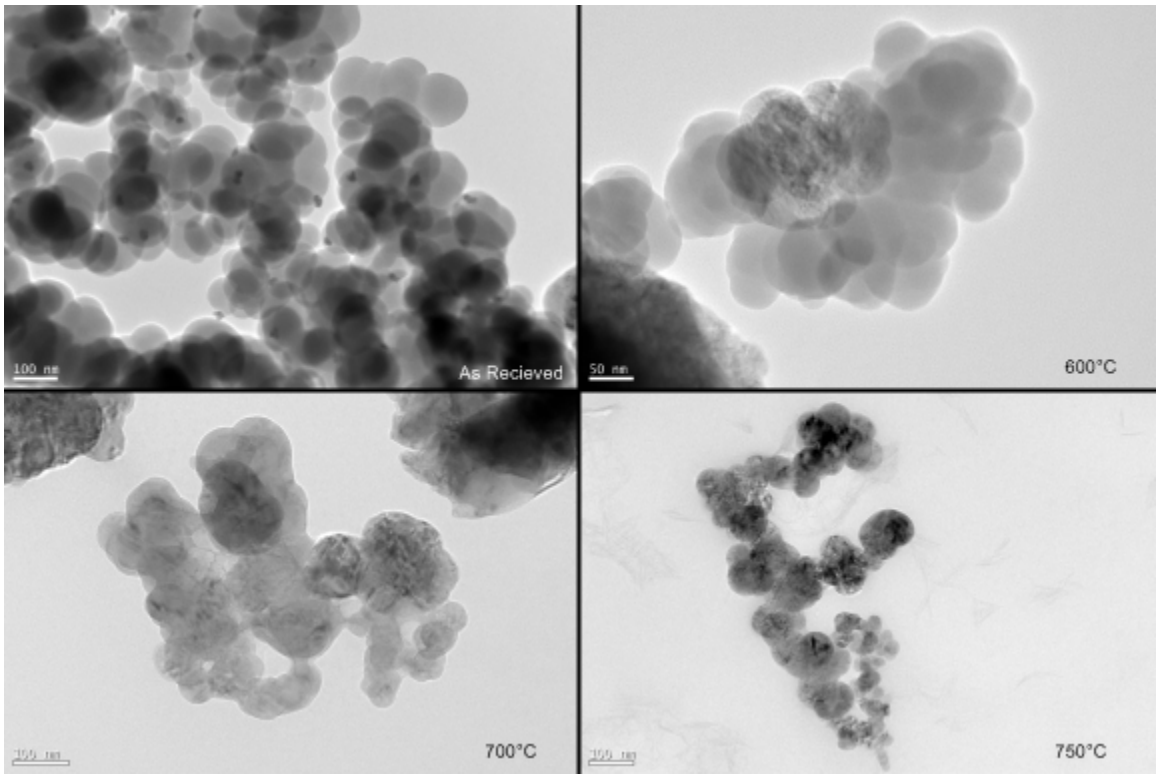

Figure 4. 4 TEM micrograph of Aerosol particles formed in a FBR under the following conditions: A) As received B) annealed at 600°C C) annealed at 700°C, and D) annealed at 750°C.

The diffusion of hydrogen is dependent on temperature, as would be expected from most diffusion process. In crystalline silicon, the activation energy of diffusion of

hydrogen at lower temperatures has been calculated to be between 2 and 5 times greater than hydrogen at higher temperatures.[17] Differences in diffusion are based on changes in the hydrogen structure inside of the silicon lattice. At lower temperatures, the arrangement with the lowest potential energy for the hydrogen is in a bonded position (Si-H). The hydrogen molecule has also been observed in areas absent of defects, but is relatively immobile at temperatures lower than 500°C. As the temperature is increased, the hydrogen bonds break and allow atomic hydrogen that can more easily move in the lattice and defect sites.[17,18] Although the ratios of hydrogen diffusion at different temperatures agree with the findings of this study, the magnitudes of activation energies are different. The activation energy of hydrogen diffusion in silicon calculated at the low temperature range in this study is only 0.5 eV, where the activation energy for the same temperatures in literature is 2.7 eV. This difference points to an alternative mechanism that controls the diffusion of hydrogen out of the particles due to the small size of the particles compared to the size of the thin films used in the reported results.

Table 4. 1 Hydrogen content (by volume) of as is and annealed samples.

Annealing Temperature	Hydrogen Content
Room temp. (no anneal)	0.0086%
400°C	0.0078%
500°C	0.0060%
600°C	0.0028%, 0.0031%
650°C	0.0026%
700°C	0.0017%
750°C	0.0022%

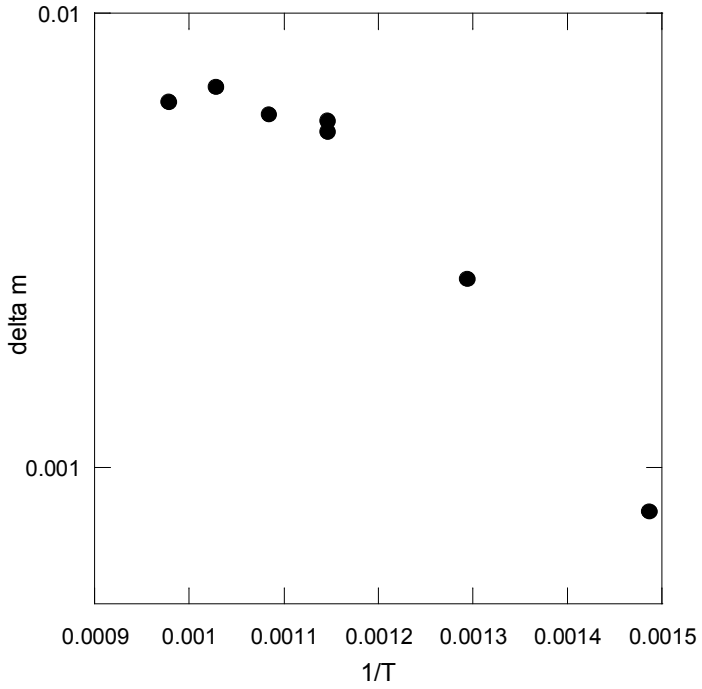

Figure 4. 5 Activation energy change near 600°C. Lower temperature energy is roughly 5 times greater than the higher temperature range.

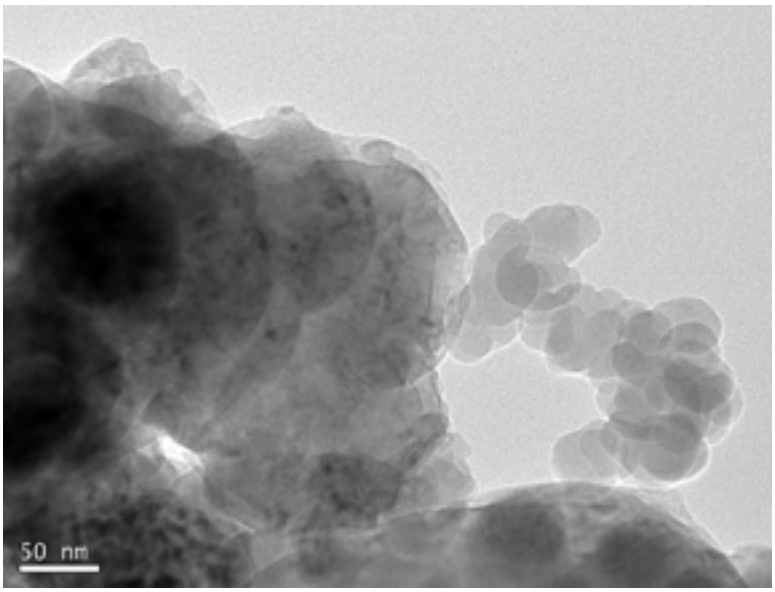

Figure 4. 6 Small amorphous particles and large crystalline particles allude to a non-diffusion limiting process.

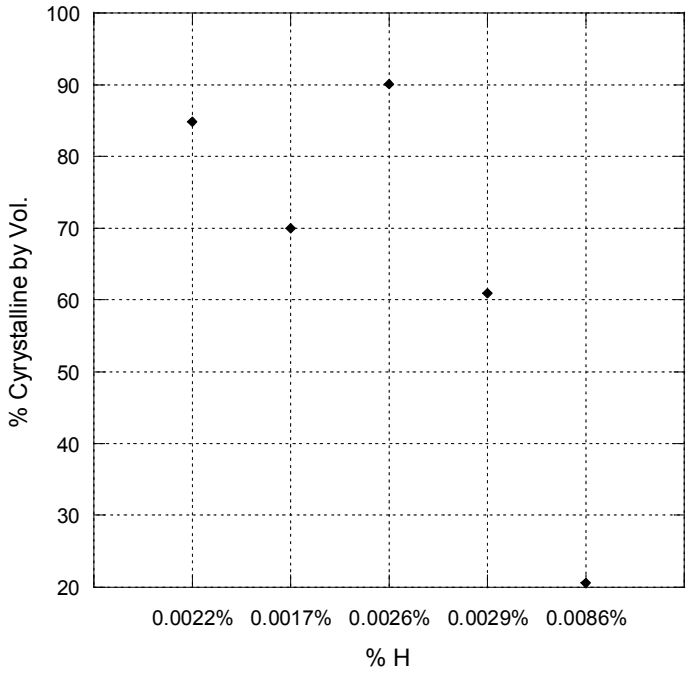

Figure 4. 7 % H vs. % Crystalline material by volume. There is a change in slope near the hydrogen content that corresponds to 600°C.

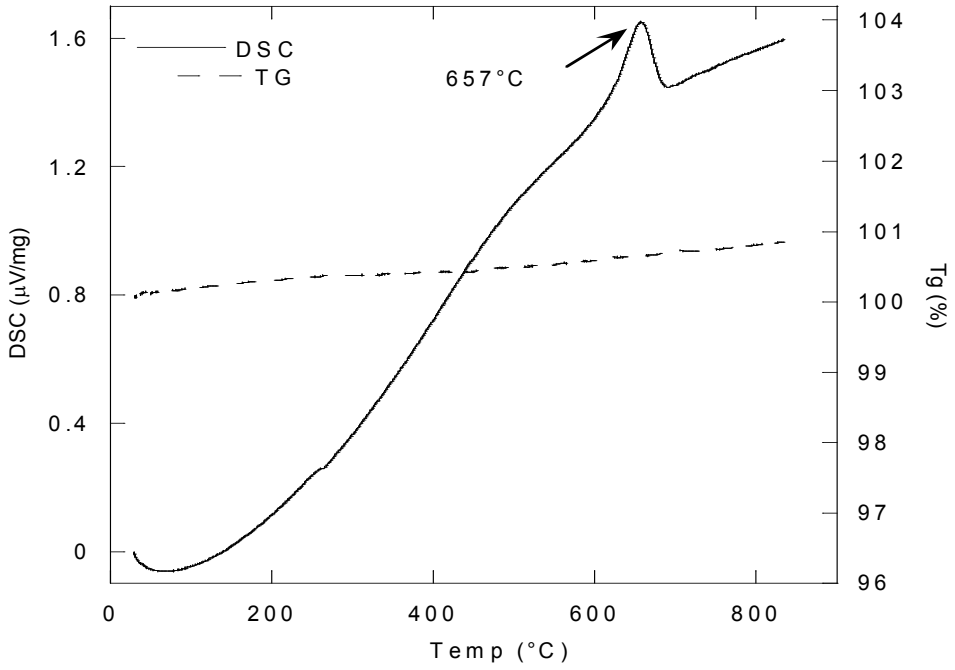

Figure 4. 8 DSC results displaying crystallization at 657°C.

It has been theorized in literature that the fines are a major contributor to the growth of the granular silicon by means of particle "scavenging".[6] This would be based on the fine particles agglomerating on the granular material as a growth mechanism, over a classical CVD model where the granular material grows layer by layer. Analysis of granular material in previous work (chapter 3) gives little indication of agglomeration of the fines material as a major contributing factor the formation of the granular silicon. Images obtained via the TEM and XRD data reveal no amorphous material which would most likely be observed if copious quantities of the aerosol particles were scavenged during granular growth. Evidence of remaining amorphous particles is given by the amorphous particles still present in samples annealed at temperatures close to that of the

reactor temperature. Additional evidence suggests that the difference in sizes of the twins between the granular material and the annealed aerosol particles could imply different processes of twinning. The larger twins in the granular material may imply a growth mechanism rather than rapid crystallization in the particles.

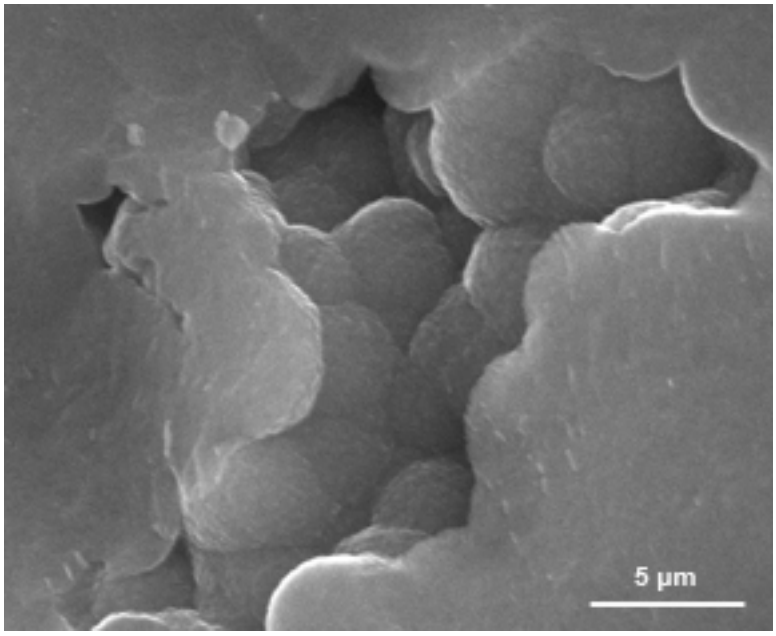

Figure 4. 9 Nano-texture on pore wall could indicate fines agglomeration on surface when less dense material is deposited.

The presence of hydrogen in the granular material observed by FTIR leaves the possibility of a small amount of aerosol trapped in the material. Close examination of the pore wall lining reveals a nano texture on order of 30 nm in diameter (Figure 4.9). There is a possibility that this is evidence of aerosol particles sticking to the surface of the granule at times where less dense material is formed instead of the grains as previously thought. Hydrogen may also be trapped inside of the silicon matrix in the tetrahedral

position or in a so-called "M" site that actually forms a three center bond with two other Si atoms of the diamond cubic structure during growth.[18]

4.4 Conclusions

The aerosol particles formed in the FBR are mostly amorphous in nature with a mean and median diameter of 78 nm. The size distribution is similar to those found in literature; however the structure of the material is debated. Hsu and colleagues found their material to be completely crystalline while Onischuk and colleagues found no evidence of crystallinity. The structure of the aerosol particles in this study shows characteristics of both studies.

Fourier transform infrared spectroscopy was used to determine chemical bond information. Signature bonds associated with hydrogenated amorphous silicon was detected at similar intensities as found in literature. Subsequent annealing techniques revealed a correlation between rising temperatures and the loss of Si-H bonds. Hydrogen analysis with a Leco hydrogen analyzer supported this evidence with a decrease in hydrogen content (by weight) as the annealing temperature is increased. In addition, as the hydrogen content is decreased, the crystallinity of the particles increases. The driving force for this change may be related to a diffusionless process. Evidence of this process is supported by TEM images of small particles remaining amorphous after larger particles have already crystallized.

A shift in activation energy for hydrogen diffusion between higher and lower temperatures has also been observed at a temperature near 600°C. The activation energy

is much higher at lower temperatures than at higher temperatures. Although similar trends have been observed in both amorphous and crystalline silicon, the magnitude of the activation energy is much less than those found in literature (1 eV in this study and .3-1.2 eV in literature for higher temperatures). Spectra from the FTIR spectrometer agree with this data; after 600°C, less Si-H bonds are present in the material.

Overall the agglomeration of fine, nm sized particles contribution to the growth of the polysilicon granules is determined to be minimal. Hydrogen present in the granules may be attributed to hydrogen entrapment during growth. Particle agglomeration on surfaces of pores may contribute very little to the hydrogen content of the granule.

4.5 References

[1] Caussat B, Hemati M, Couderc JP. Silicon deposition from silane or disilane in a fluidized bed – part II: theoretical analysis and modeling. Chem Eng Sci. **50** (1995) 3625

[2] Coso G, Canizo C, Luque A. Chemical vapor deposition model of polysilicon in a trichlorosilane and hydrogen system J Electrochem Soc. **155** (2008) D485

[3] Rohatgi NK, Hsu GC, Lutwack R. edited Dismukes JP, Erhard S, Rai-Choudhury P, Hunt LP. *Silane pyrolysis in a fluidized bed reactor*. Materials and New Processing Technologies for Photovoltaics. Proceedings volume 82-8. 1982 pg 477. The electrochemical Society, Inc. Pennington, NJ 08534

[4] Pina J, Bucala V, Schbib NS, Ege P, Lasa HI. Modeling a silicon CVD spouted bed pilot plant reactor. Int J Chem React Eng **4** (2006) 1

[5] Onischuck AA, Strunin VP, Ushakova MA, Samoilova RI, Panfilov VN. Analysis of hydrogen and paramagnetic defects in a-Si:H aerosol particles resulting from thermal decomposition of silane. Phys Stat Sol (b). **193** (1996) 25

[6] Hsu G, Hogle R, Rohatgi N, Morrison A. Fines in fluidized bed silane pyrolysis. J Electrochem Soc. **131** (1984) 660-663

[7] Onischuk AA, Strunin VP, Ushakova MA, Panfilov VN. On the pathways of aerosol formation by thermal decomposition of silane. J Aerosol Sci. **28** (1997) 207

[8] Slootman F, Parent JC. Homogeneous gas-phase nucleation in silane pyrolysis. J Aerosol Sci. **25** 1994 15

[9] Eversteijn FC. Gas-phase decomposition of silane in a horizontal epitaxial reactor. Philips Res Repts. **26** (1971) 134

[10] Qian ZM, Michiel H, Van Ammel A, Nijs J, Mertens R. Homogeneous gas phase nucleation of silane in low pressure chemical vapor deposition (LPCVD). J Electrochem Soc. **135** (1988) 2378

[11] Onishchuck AA, Levykin AI. Strunin VP, Ushakova MA, Samoilova RI, Sabelfeld KK, Panfilov VN. Aerosol Formation under heterogeneous/homogeneous thermal decomposition of silane: experiment and numerical modeling. J Aerosol Sci. **31** (2000) 879

[12] Onischuk AA, Strunin VP, Ushakova MA, Panfilov VN. Studying of silane thermal decomposition mechanism. Int J Chem Kinet. **30** (1998) 99

[13] Gupta T, Colvin VL, George SM. Hydrogen desorption kinetics from monohydride and dihydride species on silicon sufraces. Phys Rev B. **37** (1988) 8234

[14]Stefanov BB, Gurevich AB, Weldon MK, Raghavachari K, Chabal YJ. Silicon Epoxide: unexpected intermediate during silicon oxide formation. Phy Rev Letter. **81** (1998) 3908

[15]Stegner AR, Pereira RN, Klein K, Wiggers H, Brandt MS, Stutzmann M. Phosphorus doping of Si nanocrystals: Interface defects and charge compensation. Physica B. **401-402** (2007) 541

[16] McMillan JA, Peterson EM. Kinetics of decomposition of amorphous hydrogenated silicon films. J App Phys. **50B (**1979) 5238

[17] Pearton SJ, Corbett JW, Shi TS. Hydrogen in crystalline Semiconductors. App Phys A. **43** (1987) 153

[18] Change KJ, Chadi DJ. Hydrogen bonding and diffusion in crystalline silicon. Phys Rev B **40** (1989) 11644

Chapter Five: Conclusions

5.1 Concluding remarks

Fluidized bed technology is quickly becoming a popular means of producing photovoltaic grade polysilicon for the solar panel market due to low cost of operation and high quality of material that is produced. With advancing use, it becomes extremely important to characterize the product to understand growth and handling processes that can make this product more efficient to make and use.

Microscopy techniques reveal that the polysilicon is composed of a very fine (30 nm) and heavily twinned grain structure which suggests that the material was grown at a very rapid rate. Small grain sizes have also been cause for a material that is 10% less hard than single crystal silicon. However, additional heat treatments have caused abnormal grain growth at temperatures above 1050°C which may lead to a higher hardness in the material with further investigation.

Microscopy results have also led to the observation that the material is composed of evenly spaced porous rings. Evidence of changes in density between the porous rings and the bulk of the granule suggests a cyclic growth pattern. High annealing temperatures have also caused changes in the pore walls. Pore walls with rounded material protruding from the side become faceted after annealing at 1100ºC, suggesting a

change in grain growth mechanisms at these higher temperatures. Literature review supports this evidence in thin and thick film polysilicon.

Homogeneously nucleated particles have also been observed in conjunction with the polysilicon granules. The material has been studied by others to understand the growth kinetics, but little research has been performed on the material itself. Examination of the structure revealed that it is hydrogenated amorphous nano sized silicon particles. Annealing in vacuum causes the material to lose much of its hydrogen content as well as causing the material to crystallize. In addition, calculated the activation energies for hydrogen diffusion in both crystalline and amorphous silicon are much lower in these small particles than found in literature. It is still unclear as to which mechanism occurs first, hydrogen leaving or crystallization, but both appear to increase the rate of the other.

Study of the granules leaves little evidence that the aerosol particles are a large contributor to the overall growth of the granules as suggested in literature. Rather, these particles should be further examined for use as an additional product of the FRB.

Appendix

A.I Procedural Methods Details

A.I.I Gatan Model 623 Disc Grinder

Before mounting the sample onto the Gatan hand polisher, the dial must be calibrated. To calibrate, place the metal stub into the polisher and align the stub's surface with the surface of the polisher. This is accomplished by placing the apparatus face down onto a flat surface such as glass. The stub is displaced by turning the dial handle clockwise to move the stub out of the polisher and counterclockwise to move the stub into the polisher. See the user manual for alternative methods for aligning the parts. After aligning the apparatus, the large, lower dial must be turned to align the black marker with the zero marker on the hand dial. Now the polisher is calibrated to zero.

Once the user has completed side one to the desired final polish and has reached the last step on side two, it becomes necessary to monitor the thickness of the sample with the hand dial on the top of the polisher. The dial is set to read the thickness based on the distance that the metal stub is pressed inward from the polisher base. To determine the current thickness of the material, first turn the dial until the marker is aligned with zero. Then turn the dial to bring the sample's face into alignment with the polisher's surface. The approximate thickness of the sample is the value on the dial indicated near the black marker. As the thickness is decreased, it is no longer necessary to re-set the dial to zero read the value of the thickness.

A.I.II VCR Dimpler

Turn the machine "on" with the power switch located in the rear of the machine. Once the sample is in place on the mount, the dimpler parameters can be set. The force is controlled by the "force setpoint" knob. In order the view the force applied, make sure that the toggle switch below the readout window is set to "F (g)". The force should be set at no higher than 40 g for silicon. The "z offset" knob is used to set the desired thickness of the sample. The set point for this knob indicates the desired thickness to be removed from the sample, so initial thickness of the sample must be known. The machine will stop dimpling once this value has reached zero. The balance is set to zero and damping is above 7 for brittle materials such as silicon. The speed can be controlled in the lower right hand corner of the machine, and is usually set near 50. The "Arm up" and "Arm down" buttons control the arm holding the dimpler tool.

Tool 3i was used with both the 3 and 1 μm diamond solutions. Tools were kept separate to discourage contamination and scratching. The padded tool was used to help with additional damping. Earlier procedures included the use of the non-padded tools, but were discovered to promote cracks in the silicon.

A.I.III VCR Ion Mill

The copper mounted sample is placed onto the open sample holder with a small amount of grease to hold the sample on. The holder is screwed into the copper mount, and placed into the vacuum chamber. The lid is replaced onto the chamber, and the mount is turned to approximately 20°.

The program used to run the ion mill is XLA / 2000 Ion / Atom Mill. Before the ion guns are turned on, the chamber is evacuated by selecting "vacuum on" on the information panel. The voltage can then be set by typing in a numerical value between 0 and 7 kV. The rotation of the sample may also be selected; a full 360° turn is generally chosen. Next, the "vent to atmosphere" field is selected and the argon is turned on. The last step is to ensure that the knobs controlling the gas throughput located on the front of the electrical panel are fully closed. The guns are turned on by pressing "run" on the computer after the chamber has fully evacuated. The knobs are then turned slowly towards open to allow a current no more than 300 mA each to pass through the argon guns. The sample requires approximately 5 hours of milling to form a hole sufficient for viewing.